J Neurophysiol 96: 1912–1926, 2006.
First published June 28, 2006; doi:10.1152/jn.00205.2006.

Contribution of Persistent Na^+ Current and M-Type K^+ Current to Somatic Bursting in CA1 Pyramidal Cells: Combined Experimental and Modeling Study

David Golomb,[1] Cuiyong Yue,[2] and Yoel Yaari[2]

[1]*Department of Physiology and Zlotowski Center for Neuroscience, Faculty of Health Sciences, Ben-Gurion University, Be'er-Sheva, Israel; and* [2]*Department of Physiology, Institute of Medical Sciences, Hebrew University-Hadassah Faculty of Medicine, Jerusalem, Israel*

Submitted 26 February 2006; accepted in final form 21 June 2006

Golomb, David, Cuiyong Yue, and Yoel Yaari. Contribution of persistent Na^+ current and M-type K^+ current to somatic bursting in CA1 pyramidal cells: combined experimental and modeling Study. *J Neurophysiol* 96: 1912–1926, 2006. First published June 28, 2006; doi:10.1152/jn.00205.2006. The intrinsic firing modes of adult CA1 pyramidal cells vary along a continuum of "burstiness" from regular firing to rhythmic bursting, depending on the ionic composition of the extracellular milieu. Burstiness is low in neurons exposed to a normal extracellular Ca^{2+} concentration ($[Ca^{2+}]_o$), but is markedly enhanced by lowering $[Ca^{2+}]_o$, although not by blocking Ca^{2+} and Ca^{2+}-activated K^+ currents. We show, using intracellular recordings, that burstiness in low $[Ca^{2+}]_o$ persists even after truncating the apical dendrites, suggesting that bursts are generated by an interplay of membrane currents at or near the soma. To study the mechanisms of bursting, we have constructed a conductance-based, one-compartment model of CA1 pyramidal neurons. In this neuron model, reduced $[Ca^{2+}]_o$ is simulated by negatively shifting the activation curve of the persistent Na^+ current (I_{NaP}) as indicated by recent experimental results. The neuron model accounts, with different parameter sets, for the diversity of firing patterns observed experimentally in both zero and normal $[Ca^{2+}]_o$. Increasing I_{NaP} in the neuron model induces bursting and increases the number of spikes within a burst but is neither necessary nor sufficient for bursting. We show, using fast-slow analysis and bifurcation theory, that the M-type K^+ current (I_M) allows bursting by shifting neuronal behavior between a silent and a tonically active state provided the kinetics of the spike generating currents are sufficiently, although not extremely, fast. We suggest that bursting in CA1 pyramidal cells can be explained by a single compartment "square bursting" mechanism with one slow variable, the activation of I_M.

INTRODUCTION

The intrinsic discharge mode of individual cortical pyramidal cells varies along a spectrum of "burstiness," from regular firing evoked by depolarization of the neuron to spontaneous bursting unprovoked by any extrinsic stimuli (Jensen et al. 1994; Schwartzkroin 1975; for a detailed description of firing and bursting patterns, see Fig. 1 in Su et al. 2001). A large body of evidence now indicates that the propensity of a neuron to burst depends not only on its constitution, i.e., the nature and properties of ionic conductances expressed in its plasma membrane, but also on its environment, i.e., the ionic composition of the milieu in which it is embedded. Thus regular firing pyramidal cells readily convert to a bursting mode when the extracellular concentrations of Ca^{2+} ($[Ca^{2+}]_o$) or K^+ ($[K^+]_o$) decrease or increase, respectively (Jensen et al. 1994; Su et al. 2001). Such changes in extracellular ion composition accompany neuronal activity (Heinemann et al. 1977), which may explain why the propensity for bursting of pyramidal cells increases with the level of activity in their surrounds (Harris et al. 2001). Interestingly, blocking Ca^{2+} currents or Ca^{2+}-activated K^+ currents (Azouz et al. 1996; Jensen et al. 1994; Su et al. 2001) does not increase the propensity for bursting. Given that the bursting mode plays important roles in electrical signaling, normal and abnormal neuronal synchronization, and induction of long-term synaptic plasticity (Izhikevich et al. 2003; Lisman 1997; Yaari and Beck 2002), it is important to understand how constitution and environment interact in regulating this discharge mode. To date, most theoretical studies of intrinsic bursting have focused on the former factor.

In neocortical, subicular, and CA3 pyramidal cells, intrinsic bursting has been attributed to recruitment of Ca^{2+} currents by the primary Na^+ spike (Chen et al. 2005; Jung et al. 2001; Larkum et al. 1999; Metz et al. 2005; Wong and Prince 1981). In line with these experimental observations, many models of Ca^{2+} current-dependent bursting suggest a "ping-pong" interplay between fast Na^+ and K^+ currents in the soma and slow Ca^{2+} and K^+ (mostly Ca^{2+}-dependent) currents in the apical dendrites (Mainen and Sejnowski 1996; Pinsky and Rinzel 1994; Traub and Miles 1991; Traub et al. 1991, 1994; Warman et al. 1994). In adult CA1 pyramidal cells, however, bursting behavior persists after almost complete truncation of the apical dendrites (Yue et al. 2005). Therefore the mechanism of bursting in the latter neurons may be different from the ping-pong mechanism, which depends on the integrity of apical dendrites.

We study the mechanism by which changes in $[Ca^{2+}]_o$ modulate transitions between regular firing and bursting in adult CA1 pyramidal cell by combining electrophysiological, computational, and analysis techniques.

METHODS

Hippocampal slices

All animal experiments were conducted in accordance with the guidelines of the Animal Care Committees of the Hebrew University. Adult male Sabra rats were decapitated under deep isoflurane anes-

Address for reprint requests and other correspondence: D. Golomb, Dept of Physiology, Faculty of Health Sciences, Box 653, Ben-Gurion University, Be'er-Sheva 84105, Israel (E-mail: golomb@bgu.ac.il).

The costs of publication of this article were defrayed in part by the payment of page charges. The article must therefore be hereby marked "*advertisement*" in accordance with 18 U.S.C. Section 1734 solely to indicate this fact.

thesia, and transverse hippocampal slices (400 μm) were prepared with a vibrating microslicer (Leica) and transferred to a storage chamber perfused with oxygenated (95% O_2-5% CO_2) artificial cerebrospinal fluid (ACSF) containing (in mM) 124 NaCl, 3.5 KCl, 2 $MgCl_2$, 1.6 $CaCl_2$, 26 $NaHCO_3$, and 10 D-glucose, pH 7.4, osmolarity 305 mosM, where they were maintained at room temperature. Slices were placed one at a time in an interface chamber (33.5°C) and perfused with oxygenated ACSF. To truncate the apical dendrites of CA1 pyramidal cells, a deep cut was made in stratum radiatum close to and parallel to stratum pyramidale using a broken pipette or a razor blade chip propelled by a micromanipulator (Yue et al. 2005). Truncation was confirmed by recording field potentials in stratum pyramidale (see following text) before and after cutting. Orthodromic field potentials evoked by stimulating in stratum radiatum disappeared after cutting, while antidromic field potentials evoked by stimulating in alveus remained large (Yue et al. 2005). The slices were allowed to recover in the chamber for ≥1 h before initiating a recording session.

Electrophysiological recordings

Intracellular recordings were obtained using sharp glass microelectrodes containing 4 M K^+-acetate (90–110 MΩ). An active bridge circuit in the amplifier (Axoclamp 2B, Axon Instruments, Foster City, CA) allowed simultaneous injection of current and measurement of membrane potential. The bridge balance was carefully monitored and adjusted before each measurement. The intracellular signals were filtered on-line at 10 kHz, digitized at a sampling rate of ≥10 kHz, and stored by a personal computer using a data-acquisition system (Digidata 1322A) and pCLAMP software (Axon Instruments).

Drugs

Stock solutions of 4β-phorbol 12,13-dibutyrate (PDB; 10 mM), riluzole (10 mM), and phenytoin (100 mM) were prepared in dimethyl sulfoxide (DMSO) and stored at −20°C. They were usually diluted at 1:1,000 when added to the ACSFs. Control ACSFs contained equal amounts of DMSO (0.001%), which by itself had no effects on the measured parameters. All other drugs were added to the ACSFs from aqueous stock solutions. Chemicals and drugs were obtained from Sigma (Petach-Tikva, Israel).

Cell model

The somatic, single-compartment model was represented by coupled differential equations according to the Hodgkin-Huxley-type scheme. We constructed the model in two stages. In the first stage, we introduced only the ionic currents that are involved in firing dynamics in 0 $[Ca^{2+}]_o$, at which it is simpler to analyze. In the second state, we added voltage-gated Ca^{2+} and Ca^{2+}-activated K^+ currents, to explore their influence on bursting behavior.

MODEL FOR 0 $[CA^{2+}]_O$. The model includes the currents that are known to exist in the soma and proximal dendrites: the transient Na^+ current (I_{Na}) and the delayed rectifier K^+ current (I_{Kdr}) that generate spikes, and the muscarinic-sensitive K^+ current (I_M) that contributes the slow variable necessary for bursting (Bertram et al. 1995; Yue and Yaari 2004, 2006). A model with these three currents only is the minimal model that allows bursting. We added the persistent sodium current (I_{NaP}) because we wanted to focus on its contribution to bursting (Su et al. 2001; Yue et al. 2005). The A-type K^+ current (I_A) is included as well even though its density is much higher in the apical dendrites than in the soma (Hoffman et al. 1997). The current balance equation is (Borg-Graham 1999)

$$C\frac{dV}{dt} = -g_L(V - V_L) - I_{Na} - I_{NaP} - I_{Kdr} - I_A - I_M + J_{app} \quad (1)$$

where $C = 1\ \mu F/cm^2$, $g_L = 0.05$ mS/cm^2, $V_L = -70$ mV, and I_{app} is the applied current. The ionic currents are: $I_{Na}(V, h) = g_{Na}m_\infty^3(V)h(V - V_{Na})$, $I_{NaP}(V) = g_{NaP}p_\infty(V)(V - V_{Na})$, $I_{Kdr}(V, n) = g_{Kdr}n^4(V - V_K)$, $I_A(V, b) = g_A a_\infty^3(V)b(V - V_K)$, $I_M(V, z) = g_M z(V - V_K)$. The conductances and reversal potentials are: $g_{Na} = 35$ mS/cm^2, g_{NaP} varies between 0 and 0.41 mS/cm^2, $g_{Kdr} = 6$ mS/cm^2, $g_A = 1.4$ mS/cm^2, $g_M = 1$ mS/cm^2, $V_{Na} = 55$ mV, $V_K = -90$ mV. The kinetics equations and parameters are listed in Table 1. The cell model for zero $[Ca^{2+}]_o$ has five dynamical variables: V, h, n, b, and z.

MODEL FOR NONZERO $[CA^{2+}]_O$. This second model includes all the currents that belong to the first model, with the same parameters (except for the effect of $[Ca^{2+}]_o$ on θ_p, the half-maximum potential of I_{NaP}; see Table 1). In addition, we added three more ionic currents: the high-threshold Ca^{2+} current (I_{Ca}), and two Ca^{2+}-activated K^+ currents, namely, the fast Ca^{2+}-activated K^+ current (I_C), which contributes to rapid spike repolarization (Storm 1987), and the slow Ca^{2+}-activated K^+ current (I_{sAHP}), which mediates a slow afterhyperpolarization (AHP) and spike frequency adaptation (Madison and Nicoll 1984). This model includes, therefore the most importantcurrents known in somata and proximal axons of CA1 cells. The current balance equation in this variation of the model is

$$C\frac{dV}{dt} = -g_L(V - V_L) - I_{Na} - I_{NaP} - I_{Kdr} - I_A - I_M - I_{Ca} - I_C - I_{sAHP} + I_{app} \quad (2)$$

The ionic currents are: $I_{Ca}(V,r) = g_{Ca}r^2(V - V_{Ca})$, $I_C(V, c) = g_C d_\infty([Ca^{2+}]_i)c(V - V_K)$, $I_{sAHP}(V, q) = g_{sAHP}q(V - V_K)$. The conductances and reversal potentials are: g_{Ca} is typically between 0 and 0.2 mS/cm^2, $g_C = 10$ mS/cm^2, $g_{sAHP} = 5$ mS/cm^2, $V_{Ca} = 120$ mV. The kinetics equations and parameters are listed in Table 2. The dynamics of the calcium concentration inside the cell, $[Ca^{2+}]_i$ are

$$\frac{d[Ca^{2+}]_i}{dt} = -\upsilon I_{Ca} - [Ca^{2+}]_i/\tau_{Ca} \quad (3)$$

$\upsilon = 0.13$ cm^2/(ms×μA), $\tau_{Ca} = 13$ ms. The variable $[Ca^{2+}]_i$ in our model is dimensionless (Traub et al. 1994). It is proportional to the Ca^{2+} concentration in a thin internal cylindrical shell adjacent to the membrane.

The low-threshold T-type Ca^{2+} current was not included in the model because it is localized mostly in the distal apical dendrites of adult CA1 pyramidal cells (Karst et al. 1993; Thompson and Wong 1991). The hyperpolarization-activated cationic current (I_h) (Magee 1998; Vasilyev and Barish 2002) was not included in the model because its density in the soma is much lower than in the apical dendrites (Magee 1998) and because the activation kinetics of the largest component of I_h are faster than that of I_M (Maccaferri and McBain 1996; Magee 1998; Spain et al. 1987) and cannot support bursting via a mechanism based on two slow variables (Bertram et al. 1995). The apamin-sensitive, small-conductance (SK) Ca^{2+}-activated K^+ current (I_{AHP}), which can be evoked under voltage-clamp conditions in CA1 pyramidal cells (Gu et al. 2005; Stocker et al. 1999), was not included in the model. The reason for this exclusion is that in current-clamp recordings this current does not contribute appreciably to spike frequency adaptation and the medium AHP (Gu et al. 2005).

NUMERICAL METHODS. Simulations were performed using the fourth-order Runge-Kutta method with a time step of 0.05 ms implemented as a C program or within the software package XPPAUT (Ermentrout 2002), that was used also for computing bifurcation diagrams.

STIMULATION. We analyzed the firing patterns of the neuron model in response to two types of stimuli, namely, brief and prolonged square positive current pulses. In the former case, pulse duration was 3 ms, so it could evoke a spike response without interfering with spike afterpotentials (Su et al. 2001; Yue and Yaari 2004). In the latter case,

TABLE 1. *Kinetics equations and parameters for the 0 $[Ca^{2+}]_o$ model*

Current, Variable	Kinetics/Time Constant, ms	Parameters	References/ Comments
I_{Na}, m	$m = m_\infty(V)$	$\theta_m = -30$mV, $\sigma_m = 9.5$mV.	1
I_{Na}, h	$dh/dt = \phi[h_\infty(V) - h]/\tau_h(V)$	$\theta_h = -45$mV, $\sigma_h = -7$mV,	1
	$\tau_h(V) = 0.1 + 0.75 \times \{1 + \exp[-(V - \theta_{ht})/\sigma_{ht}]\}^{-1}$	$\theta_{ht} = -40.5$mV, $\sigma_{ht} = -6$mV, $\phi = 1$.	
I_{NaP}, p	$p = p_\infty(V)$	$-47\text{mV} \le \theta_p \le -41$mV, $\sigma_p = 3$mV.	2
I_{Kdr}, n	$dn/dt = \phi[n_\infty(V) - n]/\tau_n(V)$	$\theta_n = -35$mV, $\sigma_n = 10$mV,	3
	$\tau_n(V) = 0.1 + 0.5 \times \{1 + \exp[-(V - \theta_{nt})/\sigma_{nt}]\}^{-1}$	$\theta_{nt} = -27$mV, $\sigma_{nt} = -15$mV, $\phi = 1$.	
I_{Kdr}, a	$a = a_\infty(V)$	$\theta_a = -50$mV, $\sigma_a = 20$mV.	4
I_{Kdr}, b	$db/dt = [b_\infty(V) - b]/\tau_b$, $\tau_b = 15$	$\theta_b = -80$mV, $\sigma_b = -6$mV.	4
I_M, z	$dz/dt = [z_\infty(V) - z]/\tau_z$, $\tau_z = 75$	$\theta_z = -39$mV, $\sigma_z = 5$mV.	5

The activation and inactivation curves $x_\infty(V)$ are determined by the equation $x_\infty(V) = \{1 + \exp[-(V - \theta_x)/\sigma_x]\}^{-1}$ where $x = m, h, n, a, b, z$. References and comments: *1*) Fleidervish et al. (1996), Martina and Jonas (1997); Sah et al. (1998b); and Golomb and Amitai (1997). The difference between θ_m and θ_h is smaller than what is usually measured in pyramidal cell somata, partially because the activation curve of axons in pyramidal cells is shifted toward more hyperpolarized values (Colbert and Pan 2002). *2*) French et al. (1990). In the cerebellum (Kay et al. 1998) and the entorhinal cortex (Magistretti et al. 2003), these kinetics were found to be as fast as the kinetics of I_{Na} in the submillisecond regime time scale. Therefore we consider the kinetics of I_{NaP} to be instantaneous. Recent experiments in CA1 pyramidal cells show that reducing Ca^{2+} concentration leads to a significant negative shift to θ_p [Yue et al. 2005; see also Li and Hatton 1996). Therefore, θ_p is varied throughout the paper (typically between −47 mV at 0 $[Ca^{2+}]_o$ and −41 mV at physiological $[Ca^{2+}]_o$ values). *3*) Martina et al. (1998); Sah et al. (1998a); *4*) Hoffman et al. (1997); Rush and Rinzel (1995); and *5*) Halliwell and Adams (1982).

pulse duration was very long, allowing neuronal dynamics to reach steady-state behavior (mathematically, converging to an attractor). There were also conditions in which the neuron model fired spontaneously without application of positive currents.

FIRING PATTERNS. Depending on the model parameters, the neuron model might fire in one of two patterns when stimulated with prolonged positive current pulses. *1*) Regular, tonic firing, in which neurons fired solitary spikes in a periodic manner. Often, two distinct types of tonic firing were observed: low-frequency tonic firing at frequencies of up to ~5 Hz; and high-frequency tonic firing, in which neurons fired continuously at ~100 Hz. *2*) Rhythmic bursting, in which sequential bursts were separated by periods of neuronal quiescence, typically lasting several hundreds of milliseconds. Rhythmic bursting was either periodic or aperiodic (chaotic) (Terman 1992).

BURSTING. In this study, we defined a burst as a tight cluster (inter-spike interval in the order of 10 ms) of two or more spikes generated alone (as in the case of bursts evoked by brief stimuli) or distinctly separated from the following spikes (as in the cases of spontaneous bursting or bursting evoked by prolonged stimuli). In the cases of prolonged or spontaneous activity, we quantified bursting behavior at long times (after the dynamics has converges to an attractor), namely after transient effects of the initial conditions have decayed. The average number of intraburst spikes (N_S) was computed by averaging the number of spikes per burst during a 1.5-s period 1 s after stimulus onset (i.e., after the dynamics has converged to an attractor) and rounding up this average to the closest integer. Doublet states were particular cases of periodic bursting states in which the neuron model fired exactly two spikes in a burst, namely, $N_S = 2$ (Mandelblat et al. 2001). Clearly, in regular spiking cells $N_S = 1$.

Fast-slow analysis

We used the fast-slow method (Bertram et al. 1995; Hoppensteadt and Izhikevich 1997; Izhikevich 2000, 2006; Rinzel and Ermentrout 1998) to study the bursting mechanism, to determine the role of the currents I_{NaP} and I_M in the dynamics, and to determine the necessary conditions for bursting. This method has been applied successfully to analyze periodic bursting of various biophysical models of neurons (e.g., Mandelblat et al. 2001). We applied the method for the case $[Ca^{2+}]_o = 0$ (and thus $\theta_p = -47$ mV and $g_{Ca} = 0$) because it has simpler dynamics. The analysis is based on separating the dynamical variables of the system into two subsystems, "fast" and "slow." The model has five dynamic variables: V, h, n, b, and z. The first four variables are considered to be "fast" and belong to the fast subsystem. The variable z is considered to be "slow." The analysis is exact in the limit $\tau_z \to \infty$, where τ_z is the time constant of z. It describes an approximation of the dynamics for large but finite τ_z. In the first stage of the analysis, the bifurcation diagram of the fast subsystem was computed with the slow variable z considered as a parameter. In the second stage, the dynamics of z itself were computed using the time-averaged values of the fast subsystem.

If the dynamics of the fast subsystem converges to a stable rest state (fixed point), V is determined by its value for the fixed point of the fast subsystem for the instantaneous value of z, denoted by $V_{rest,fast}(z)$, whereas z evolves slowly (Table 1). If $z_\infty[V_{rest,fast}(z)] > z$, z increases

TABLE 2. *Kinetics equations and parameters for the non-zero $[Ca^{2+}]_o$ model*

Current, Variable	Kinetics/Activation	Time Constant, ms	Parameters	References/ Comment
I_{Ca}, r	$dr/dt = [r_\infty(V) - r]/\tau_r$	$\tau_r = 1$	$\theta_r = -20$mV,	1
	$r_\infty(V) = \{1 + \exp[-(V - \theta_r)/\sigma_r]\}^{-1}$		$\sigma_r = 10$mV	
I_C, c, d	$dc/dt = [c_\infty(V) - c]/\tau_c$	$\tau_c = 2$	$\theta_c = -30$mV,	2
	$d = d_\infty([Ca^{2+}]_i)$		$\sigma_c = 7$mV,	
	$c_\infty(V) = \{1 + \exp[-(V - \theta_c)/\sigma_c]\}^{-1}$		$a_c = 6$	
	$d_\infty([Ca^{2+}]_i) = (1 + a_c/[Ca^{2+}]_i)^{-1}$			
I_{sAHP}, q	$dq/dt = [q_\infty([Ca^{2+}]_i) - q]/\tau_q$	$\tau_q = 450$	$a_q = 2$	2
	$q_\infty([Ca^{2+}]_i) = (1 + a_q^4/[Ca^{2+}]_i^4)^{-1}$			

References and comments: *1*) Kay and Wong (1987) and *2*) Lancaster and Adams (1986). The current I_C is fast and is controlled by both V and $[Ca^{2+}]_i$, whereas I_{sAHP} is slow and is controlled by $[Ca^{2+}]_i$ only.

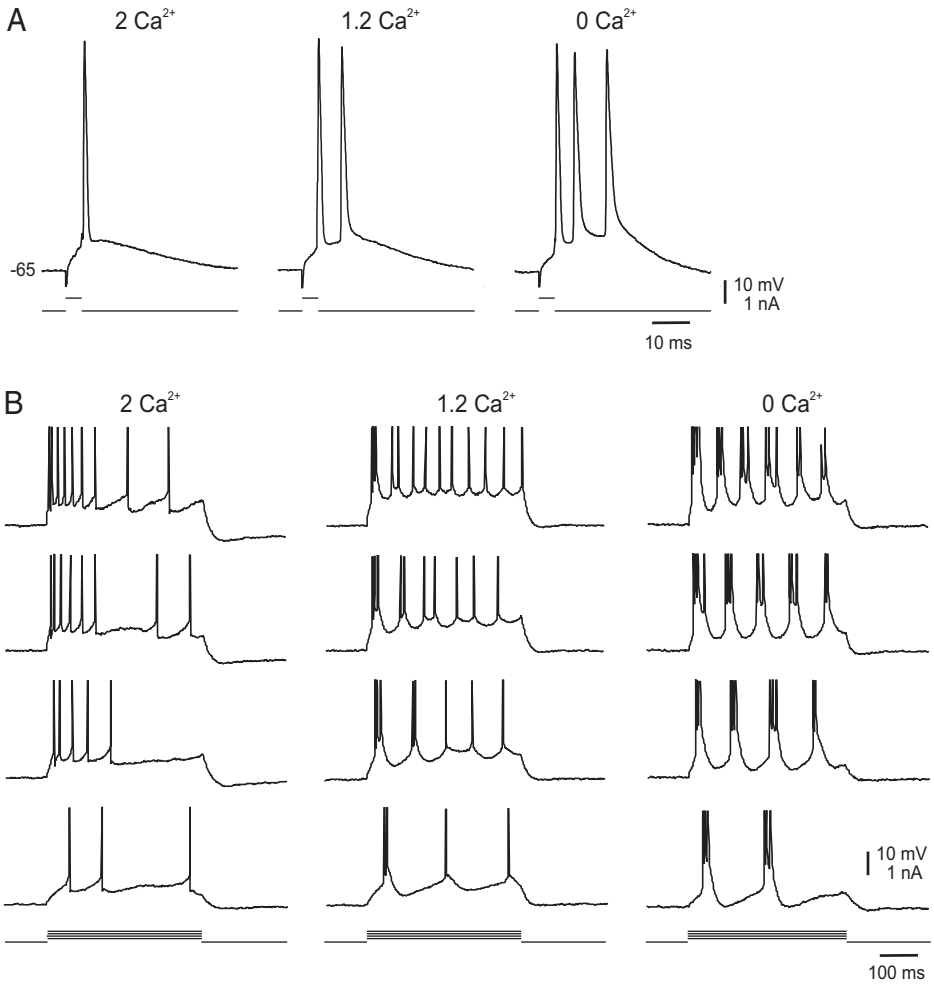

FIG. 1. Effects of lowering $[Ca^{2+}]_o$ on the firing mode of a truncated CA1 pyramidal cell. *A*: in normal artificial cerebrospinal fluid (ACSF; 2 mM Ca^{2+}) the neuron fired a solitary spike in response to suprathreshold brief depolarizing current pulses (*left*). Sequentially lowering $[Ca^{2+}]_o$ to 1.2 mM (*middle*) and to nominally 0 mM (*right*) caused spike afterdepolarization (ADP) augmentation which converted the single spike response to a burst of 2 and 3 spikes, respectively. *B*: stimulating with longer (180 ms) depolarizing current pulses of increasing intensity induced repetitive firing. In normal ACSF, the neuron generated an accommodating train of independent spikes (*left*). Reducing $[Ca^{2+}]_o$ to 1.2 and to nominally 0 mM converted these responses to repetitive bursting with much less adaptation (*middle and right*).

slowly, and if $z_\infty[V_{rest,fast}(z)] < z$, z decreases slowly. If, for a certain value of z denoted by z_{FP}, $z_\infty[V_{rest,fast}(z_{FP})] = z_{FP}$, namely, the line representing the stable rest state, $V_{rest,fast}(z)$, intersects with $z_\infty(V)$, the activation carve of z (Table 1), the point $[V_{rest,fast}(z_{FP}), z_{FP}]$ represents a fixed point of the full system. It is stable if $dV_{rest,fast}(z)/dz < [dz_\infty(V)/dV]^{-1}$. The dynamics of the fast subsystem may converge also to a stable tonic firing state (limit cycle), where T_z is the time period of the cycle that depends on z. The approximation that τ_z is much larger than the other time scales in the system, and, specifically, $\tau_z > T_z$, means that z does not vary significantly during one cycle of the fast subsystem. Therefore we can average the dynamical equation for dz/dt (Table 1) over one cycle of the fast, tonic firing to obtain (Bertram et al. 1995; Izhikevich 2006; Mandelblat et al. 2001)

$$\left\langle \frac{dz}{dt} \right\rangle = [z_\infty(V_{equiv}) - z]/\tau_z \quad (4)$$

where $\langle \ldots \rangle$ denotes time average over a period T_z and V_{equiv} is defined implicitly by the equation

$$z_\infty(V_{equiv}) = \frac{1}{T_z}\int_0^{T_z} z_\infty(V(t))dt \quad (5)$$

In the slow time scale, we can replace $\langle dz/dt \rangle$ by dz/dt. Therefore the dynamics of the slow variable z is determined, on average, by the right hand side of *Eq. 5*. If $z_\infty[V_{equiv}(z)] > z$, z increases slowly, and if $z_\infty[V_{equiv}(z)] < z$, z decreases slowly. We consider the case where, for a certain value of z denoted by z_{LC}, the line representing $V_{equiv}(z)$ intersects with the activation carve of z, $z_\infty(V)$, namely $z_\infty[V_{equiv}(z_{LC})] = z_{LC}$. In this case, the point $(V_{equiv}(z_{LC}), z_{LC})$ represent a limit cycle of the full system. It is stable if $dV_{equiv}(z)/dz < [dz_\infty(V)/dV]^{-1}$. In particular, the limit cycle is stable if the slope of $V_{equiv}(z)$ at $z = z_{LC}$ is negative.

RESULTS

Effects of lowering $[Ca^{2+}]_o$ on truncated CA1 pyramidal cells

We have recorded from 24 CA1 pyramidal cells after truncation of their apical dendrites. When activated with brief (3–4 ms) depolarizing current pulses, truncated neurons displayed normal spikes followed by a distinct, albeit variable in size, afterdepolarization (ADP; Fig. 1*A*, *left*). The mean (±SE) resting potential, apparent input resistance, and spike amplitude of these neurons were −67.8 ± 0.5 mV (range, −75 to −61 mV), 40.1 ± 2.0 MΩ (range, 20.5 to 48.7 MΩ), and 92.1 ± 5.7 mV (range, 71.7 to 103.2 mV), respectively. These values are well within the values obtained for intact neurons (Yue and Yaari 2004; Yue et al. 2005) and indicate that despite the damage inflicted by the cut and loss of most apical dendrites, the electrophysiological properties of the axo-soma are well preserved. When activated with prolonged (200 ms) depolarizing current pulses of increasing intensities, the neurons discharged repetitively and displayed spike frequency adaptation (Fig. 1*B*, *left*). Like in intact neurons (Su et al. 2001; Yue et al. 2005), approximately half of the neurons were

nonbursters and the other half were mostly high-threshold bursters (bursting only in response to long depolarizing current pulses of 2–3 times threshold intensity) with a small subset of low-threshold bursters (bursting in response to threshold-straddling stimuli).

In all 24 truncated neurons examined, lowering $[Ca^{2+}]_o$ from 2 to nominally 0 mM caused a progressive increase in the spike ADP. In 19 of these neurons (79.2%), the increase in spike ADP culminated in a high-frequency burst of three to six spikes as their minimal response to threshold depolarization (Fig. 1*A*). Lowering $[Ca^{2+}]_o$ also reduced spike frequency adaptation (Fig. 1*B*). These effects are similar to those described previously in intact neurons (Azouz et al. 1996; Su et al. 2001). Thus functional apical dendrites are not required for the expression of bursting behavior in low $[Ca^{2+}]_o$.

In nominally Ca^{2+}-free ACSF, many of the neurons converted to bursting mode manifested rhythmic bursting at their native resting potential (see following text, Fig. 4*A*) or at more depolarized potentials. Increasing the depolarizing current intensity enhanced the frequency of bursting without strongly affecting the shape of individual bursts. However, at the higher frequencies of bursting, the number of intraburst spikes progressively decreased with time (Fig. 1*B*, *right*).

Effects of blocking persistent Na^+ current

A previous study in intact CA1 pyramidal cells concluded that the augmented spike ADPs and bursting behavior in low $[Ca^{2+}]_o$ are driven predominantly by persistent Na^+ current (I_{NaP}) (Su et al. 2001). To extrapolate this finding to truncated neurons, we tested the effects of the I_{NaP} blocker riluzole (Yue et al. 2005) on bursting induced by low $[Ca^{2+}]_o$ in five such neurons. Riluzole (10 μM) blocks I_{NaP} in CA1 pyramidal cells almost completely while exerting a lesser effect on the transient Na^+ current (Spadoni et al. 2002; Urbani et al. 2000; Yue et al. 2005). Representative results are shown in Fig. 2. Adding 10 μM riluzole to the ACSF abolished low Ca^{2+}-induced bursting (Fig. 2*A*) and converted rhythmic bursting during prolonged depolarizations to regular firing (Fig. 2*B*). Similar results were obtained (data not shown) with 100 μM phenytoin ($n = 3$) and 5 μM PDB ($n = 2$), which also block I_{NaP} (Cantrell et al. 1996; Chao and Alzheimer 1995; Yue et al. 2005). Together, these data strongly suggest that bursting in low $[Ca^{2+}]_o$ is driven predominantly by I_{NaP}.

Effects of blocking M-type K^+ current

Because inactivation of I_{NaP} in CA1 pyramidal cells is very slow (in the order of seconds) (French et al. 1990), burst termination likely involves activation of an outward K^+ current. In nominally Ca^{2+}-free ACSF, Ca^{2+}-activated K^+ currents are inoperative. Hence a likely candidate for burst termination in this condition is the M-type K^+ current (I_M), previously shown to activate during the spike ADP and repolarize the neuron back to its resting potential (Yue and Yaari 2004). We tested this notion using linopirdine and XE991, selective blockers of I_M (Schnee and Brown 1998; Wang et al. 1998). Representative results from one truncated neuron bathed in Ca^{2+}-free ACSF are shown in Fig. 3. When activated by brief depolarizing pulses, the neuron generated a burst of three spikes (Fig. 3*A*, *left*). Adding 10 μM linopirdine to the Ca^{2+}-free ACSF markedly prolonged the burst and delayed repolarization of the neuron for several hundreds of milliseconds (Fig. 3*A*, *middle*). Both the primary burst and the underlying plateau potentials were readily suppressed by subsequent addition of 10 μM riluzole to the ACSF (Fig. 3*A*, *right*), suggesting that they are driven by I_{NaP}. Similar results were obtained when the neuron was stimulated with prolonged depolarizing current pulses that induced rhythmic bursting (Fig. 3*B*, *left*). Under the influence of linopirdine, rhythmic bursting converted to a plateau depolarization that lasted throughout the period of stimulation (Fig. 3*B*, *middle*). Again, adding 10 μM riluzole to the ACSF suppressed the initial burst responses and the plateau depolarizations and imposed a regular firing mode (Fig. 3*B*, *right*). Similar results were obtained in five truncated neurons treated with 10 μM linopirdine and two truncated neurons treated with 3 μM XE991. Together these data suggest that bursting in truncated neurons bathed in Ca^{2+}-free ACSF is due to interplay between I_{NaP} and I_M.

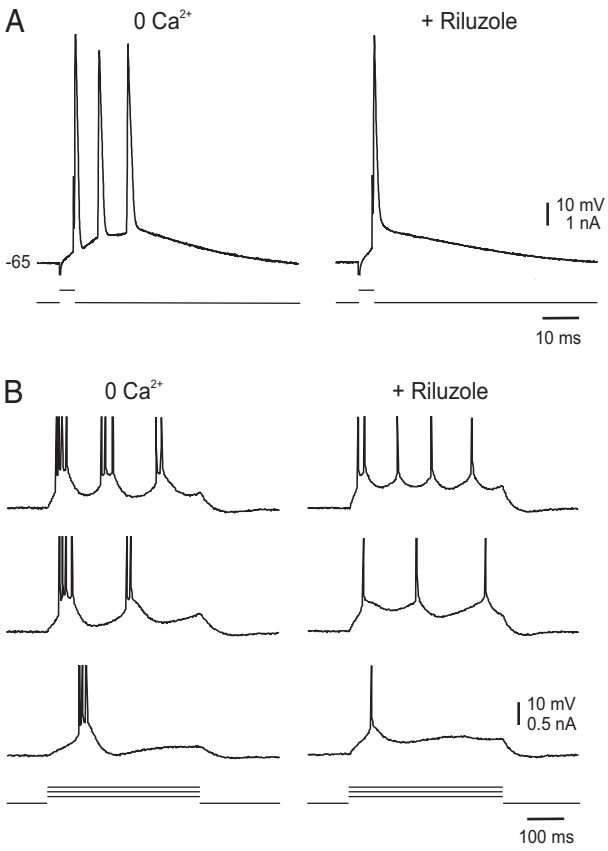

FIG. 2. The I_{NaP} blocker riluzole suppresses bursting in nominally 0 $[Ca^{2+}]_o$. *A*: exposing this truncated neuron to nominally 0 Ca^{2+} ACSF converted it to a low-threshold bursting mode (*left*). Adding 10 μM riluzole to the ACSF suppressed bursting within 24 min of exposure (*right*). *B*: in the same neuron, repetitive bursting evoked by long depolarizing current pulses (*left*) was converted to a regular firing mode by riluzole (*right*).

Construction of an experimentally based model

We have constructed a model of CA1 pyramidal cells to further understand the mechanisms underlying their somatic bursting. The results of the model are compared with the experimental results from the following aspects. First, can the model account for the variant firing patterns observed experimentally as its parameters are varied? Second, do the propen-

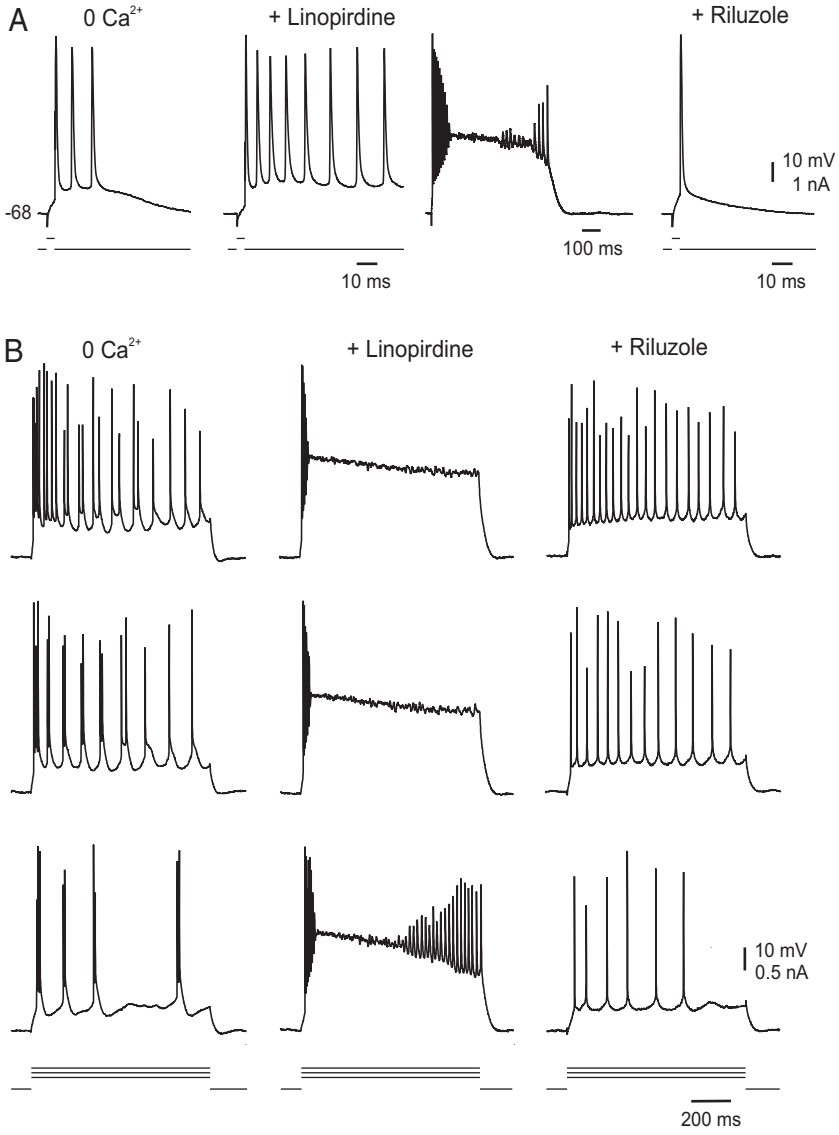

FIG. 3. The I_M blocker linopirdine converts repetitive bursting in nominally 0 $[Ca^{2+}]_o$ to plateau depolarizing potentials. *A*: exposing this truncated neuron to nominally 0 Ca^{2+} ACSF converted it to a low-threshold bursting mode (*left*). Exposing the neuron to 10 μM linopirdine for 20 min converted the 3-spike burst to a prolonged burst followed by a sustained depolarizing lasting hundreds of milliseconds (*middle* and *inset*). The burst and associated plateau depolarization were readily suppressed by subsequent addition of 10 μM riluzole (*right*). *B*: in the same neuron, repetitive bursting evoked by long depolarizing current pulses (*left*) was converted to a sustained plateau potential (*middle*), which was converted to a regular firing by riluzole (*right*).

sity for bursting and N_S vary in a similar manner in the model and in the experiments as I_{app}, g_{NaP}, or g_M vary? Finally, are the influences of g_{Ca}, g_C, and $[Ca^{2+}]_o$ on the propensity for bursting and N_S similar in the model and in the experiments? We have included in the model neuronal dynamics with only two time scales, namely that of spikes (a few milliseconds) and that of bursting (~100 ms). Experimentally, we found that many CA1 pyramidal cells also exhibited very slow dynamics (>1 s) that may cause rhythmic bursting to change eventually to repetitive spikes (Figs. 1*B*, *middle,* and 3*B*, *left*, *2 top traces*). The very slow dynamics, however, often reached a steady state. In those cases, the neurons displayed rhythmic bursting continuously, as shown in Fig. 4*A*. Therefore we omitted the very slow dynamics from the model, allowing it also to manifest rhythmic bursting (Fig. 4*B*).

Fast-slow analysis of the necessary conditions for bursting and the roles of I_{NaP} and I_M

We have shown in the preceding text that two currents, namely I_{NaP} and I_M, play essential roles in bursting in truncated CA1 pyramidal cells bathed in 0 $[Ca^{2+}]_o$. The I_{NaP} is considered here to be nonactivating (at the relevant time scales), and its activation variable, p, is considered to be instantaneous and equal to $p_\infty(V)$. The activation variable of I_M, z, is relatively slow, with time constant $\tau_z = 75$ ms. Therefore we used the fast-slow method in the condition that z is the only slow variable.

To illuminate the contribution of I_{NaP} to bursting, we carried out the analysis for four values of g_{NaP}: 0 (Fig. 5*A*), 0.2 mS/cm^2 (Fig. 5*B*), 0.3 mS/cm^2 (Fig. 5*C*), and 0.41 mS/cm^2 (Fig. 5*D*). In all panels, the bifurcation diagrams of the fast subsystem are computed with z considered as a parameter. The steady state (fixed point; thin black line) is stable for large z. This stable rest state coalesces with an unstable state and ceases to exist in a saddle-node bifurcation. The rest state is stable again for negative values of z (negative z values do not have physiological meaning, but they are important for a complete mathematical analysis). At the z value where the high rest state gains its stability (a Hopf bifurcation that is out of the scale in Fig. 5, *A* and *B*), an oscillatory state (limit cycle) emerges, corresponding to tonic, periodic firing. This oscilla-

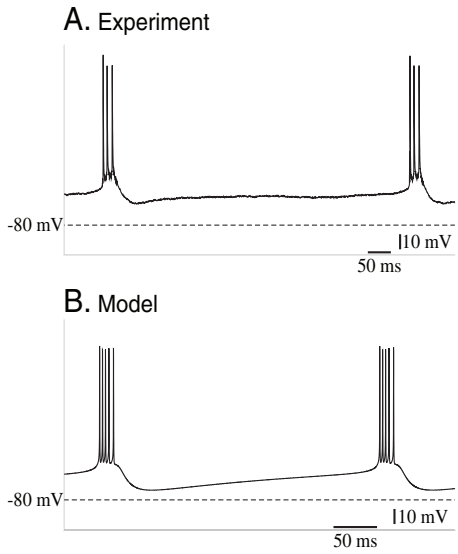

FIG. 4. Comparison of spontaneous rhythmic bursting in a truncated CA1 pyramidal cell and in the neuron model. *A*: experiment. In this truncated neuron, perfusing the slice with nominally Ca^{2+}-free ACSF induced spontaneous rhythmic bursting. *B*: modeling. An example of spontaneous bursting (I_{app} = 0 μA/cm^2) in the neuron model at $[Ca^{2+}]_o = 0$. Other parameters are: g_{NaP} = 0.3 mS/cm^2, V_L = −62 mV.

tory state extends toward the right. For $g_{NaP} = 0$ (*A*), the oscillatory state is the only stable state for small (positive) z values, and the rest state is the only stable state for larger z values. There is a tiny regime of bistability where both states are stable, but for our description, it can be ignored. For g_{NaP} = 0.2 mS/cm^2 (*B*), the bistable regime, in which both the rest state and the oscillatory state exist and are stable, is more extended. For g_{NaP} = 0.3 mS/cm^2 (*C*), the oscillatory solution extends toward the right, coalesces with an unstable periodic state, and this unstable state coalesces with another stable oscillatory state with a larger amplitude. For g_{NaP} = 0.41 mS/cm^2 (*D*), the Hopf bifurcation point is shifted to the right, and there is bistability between a rest state and a depolarized plateau. The stable oscillatory state with large amplitude almost disappears, and the amplitude of the remaining oscillatory state is small.

We then analyzed the behavior of the full system of equations defining the neuronal dynamics. For $g_{NaP} = 0$ (Fig. 5*A*), the bistable regime is tiny and cannot generate bursting states with the present kinetics of z; the neuron fires tonically. For g_{NaP} = 0.2 mS/cm^2 (Fig. 5*B*), there is a significant bistable regime. When the neuron fires, z slowly increase until it reaches beyond the bistable regime. The neuron dynamics goes to the rest state, where z decreases. When z reaches the "knee" where the stable rest state disappears, the dynamics goes back to the firing state and a new bursting cycle begins. Similar behavior occurs for g_{NaP} = 0.3 mS/cm^2 (Fig. 5*C*) except that the number of spikes (N_S) increases because of the more extended bistable regime. The system does not settle into the fast oscillations with small amplitude for this parameter value. For g_{NaP} = 0.41 mS/cm^2 (Fig. 5*D*), the system first settles into the high plateau, and the amplitude of the oscillations decreases with time. As z increases, the state switches to the fast oscillations with small amplitude, and the amplitude of the oscillations increases with time until the system switches to the rest state. This scenario leads to bursting state with fast, low-amplitude spikes whose amplitude first decreases and then increases with time (see following text, Fig. 8*B*, III).

From the fast-slow analysis, we derive several conclusions regarding the neuronal firing dynamics.

1. BISTABILITY OF THE FAST SUBSYSTEM. The bursting mechanism in our model depends on the bistability of the fast subsystem. To obtain bistability, there should be strong-enough inward current that is active in *steady state* at membrane potentials around spike threshold, namely $[g_{Na}m_\infty^3(V)h_\infty(V) + g_{NaP}p_\infty(V)]\times(V - V_{Na})$ should be large enough for V around spike threshold. In our model, this inward current can be generated by I_{NaP} or the window I_{Na}. In addition, the minimal voltage of the fast subsystem during the tonic state should be depolarized enough (above the thin dotted black line representing the unstable rest state). Therefore the kinetics of the currents underlying spike depolarization and repolarization (I_{Na} and I_{Kdr} in our model) should be fast enough (Bertram et al. 1995). Indeed, a previous model in which h and n were 3.7 times slower than in the present model that did not display bursting behavior (Golomb and Amitai 1997). If the kinetics of these variables are too fast, however, the fast subsystem will exhibit a high plateau depolarization As a result, the neuronal voltage will oscillate between a rest state and a high plateau depolarization instead of exhibiting bursts of spikes.

2. STRENGTH OF g_{NaP}. The effect of I_{NaP} on the tonic state is larger than its effect on the rest state because this current is activated at depolarized membrane potentials (Table 1). As g_{NaP} increases, the tonic state is shifted more to the right

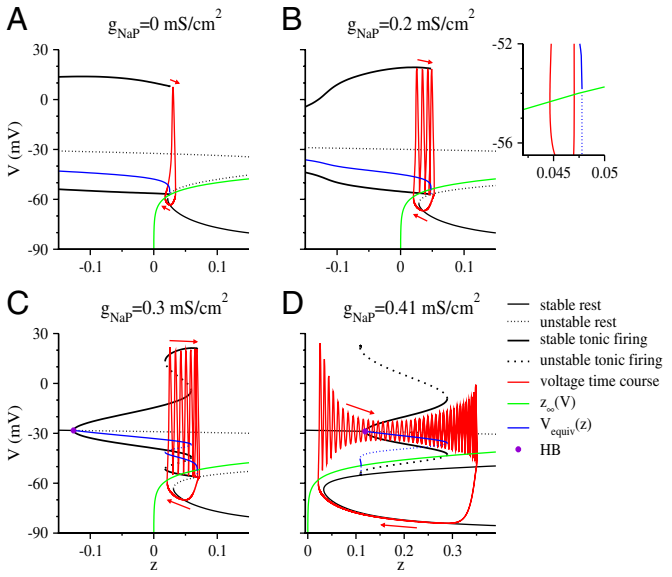

FIG. 5. Theory: fast-slow analysis of the neuronal firing patterns. Bifurcation diagrams of the fast subsystems are plotted with z considered as a parameter for $g_{NaP} = 0$ (*A*), g_{NaP} = 0.2 mS/cm^2 (*B*), g_{NaP} = 0.3 mS/cm^2 (*C*), and g_{NaP} = 0.41 mS/cm^2 (*D*); I_{app} = 1 μA/cm^2. Solid lines denote stable states and dotted lines denote unstable states. Thin black lines denote rest state, and thick black lines denote the minimal and maximal voltages of periodic, tonic firing states (limit cycles). The green curve denotes the curve $z = z_\infty(V)$ (Table 1). The blue curve denotes the value of V_{equiv} (*Eq. 5*) during periodic firing. Violet solid circles denote Hopf bifurcations. The voltage time course of the neuron in the full system (including z as a variable) is denoted by the red curve. Red arrow denotes the direction of that curve in the z–V plane.

(toward larger values of z) than the rest state. Hence the bistable regime expands as g_{NaP} increases. This regime may even be produced by increasing g_{NaP} if it had not existed for $g_{NaP} = 0$. This means that elevating g_{NaP} may induce bursting behavior and increase N_S. Increasing g_{NaP} also shifts the Hopf bifurcation of the depolarized plateau potential to the right (compare Fig. 5, *A–D*). Therefore when g_{NaP} is very large, the active phase of the burst becomes a high plateau depolarization or a sequence of low-amplitude fast spikes converging to a high plateau depolarization rather than full-blown spikes (Fig. 5*D*).

3. ACTIVATION CURVE OF I_M. To allow bursting behavior the activation curve of I_M, $z_\infty(V)$, should be located between the rest state curve and the curve of V_{equiv} (Bertram et al. 1995). If $z_\infty(V)$ is shifted toward more depolarized levels, (θ_z, the half-maximum potential of I_M, increases), the neuron will fire tonically. If $z_\infty(V)$ is shifted toward more hyperpolarized levels (θ_z decreases), the neuron will be quiescent at rest.

4. STRENGTH OF g_M. I_M is proportional to $g_M \times z$. For $g_M = 0$ (equivalent to $z = 0$ in Fig. 5, *A–D*), the neuron fires tonically or reaches a high plateau depolarization when g_{NaP} is very large. Increasing g_M is equivalent to compressing the bifurcation diagram of the fast subsystem along the z axis in Fig. 5, without modifying the kinetics of the slow variable z. Therefore as g_M increases, the slow variable z spends less time in the oscillatory state and N_S decreases. When N_S decreases to 1, the neuron fires in a tonic pattern. For very large g_M, the rest state of the fast subsystem intersects with the activation curve of z, and the neuron becomes quiescent at rest.

SUMMARY OF NECESSARY CONDITIONS FOR BURSTING. Our analysis reveals four necessary conditions for bursting. All these conditions demand that certain parameters will be in particular ranges. *1*) The kinetics of the variables underlying spike generation (inactivation of I_{Na} and activation of I_{Kdr}) should be fast enough (otherwise, there will be no bistability and the neuron will fire continuously) but not be too fast (to prevent a plateau depolarization). *2*) The fast subsystem should show bistability, and g_{NaP} supports bistability. Therefore g_{NaP} should be strong enough to generate bistability unless this bistability has already been generated by the window I_{Na}. If g_{NaP} is too strong, however, the neuron model will manifest very fast spiking with small amplitude or a plateau depolarization. *3*)The half-maximum potential of I_M, θ_z, should not be too depolarized (at which condition the neuron will fire tonically) or too hyperpolarized (at which condition the neuron will be at resting potential). *4*) g_M should be strong enough (otherwise, the neuron will fire in a regular mode or will display a high plateau depolarization) but not too strong (otherwise, the neuron will fire in a regular mode or will not fire at all).

The analysis is carried out in the limit that τ_z is much larger than all the other time constants, even though in reality it is not extremely large ($\tau_z = 75$ ms). Therefore it is necessary to examine whether the conditions for bursting obtained using the analysis are still valid for this value of τ_z. In the following subsections, we turn back to the full system and study it using numerical simulations. We also examine whether the model can account for the variant firing patterns of CA1 pyramidal cells.

Effects of varying g_{NaP}

CA1 pyramidal cells perfused with Ca^{2+}-free ACSF display a diversity of firing patterns, ranging from regular firing to spontaneous rhythmic bursting (Figs. 1–3 and 4*A*) (Azouz et al. 1996; Su et al. 2001). We first tested the hypothesis that a variation in the density of persistent Na^+ channels may generate such diversity. We assumed that in this condition $\theta_p = -47$ mV and examined the consequences of increasing g_{NaP}. When g_{NaP} was set to zero, the neuron fired in a regular mode during sustained depolarization (Fig. 6*A*). As g_{NaP} was raised, the propensity for bursting increased, so that at $g_{NaP} = 0.08$ mS/cm^2, the neuron became a periodic burster when strongly depolarized (Fig. 6*B*) and at $g_{NaP} = 0.18$ mS/cm^2, it burst-fired periodically in response to all suprathreshold stimuli (Fig. 6*C*). Further increasing g_{NaP} to 0.3 mS/cm^2 increased the burstiness of the neuron, so it now fired a burst also in response to brief stimuli (Fig. 6*D*). Changing V_L from -70 to -62 mV destabilized the rest state and caused spontaneous rhythmic bursting when g_{NaP} was high (Fig. 4*B*). For $g_{NaP} = 0$, the neuron was quiescent even for $V_L = -62$ mV.

In all the cases shown in Figs. 4*B* and 6, the number of spikes in the first burst was larger than or equal to N_S, the average number of spikes in later bursts. The reason for that is that z, the activation variable of I_M, is nearly zero at the beginning of the stimulus but increases later, so the limiting effect of I_M on the number of spikes is expressed with a delay.

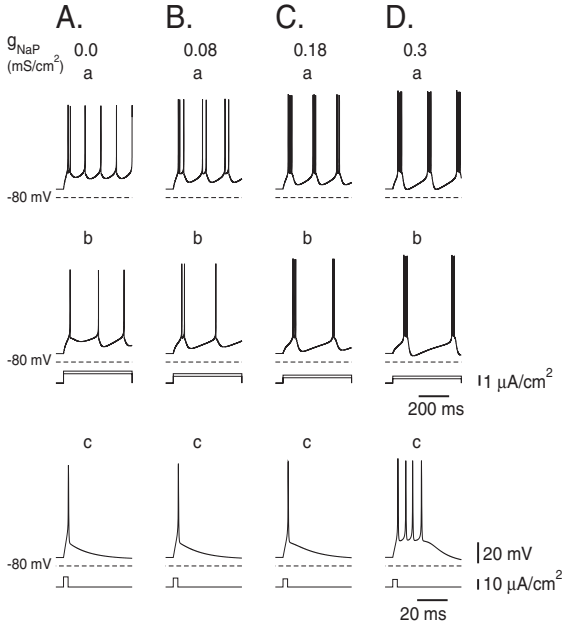

FIG. 6. Modeling: variant firing patterns of the neuron model for $[Ca^{2+}]_o = 0$ and various values of g_{NaP}. *A–D* correspond to the following values of g_{NaP} (in mS/cm^2): 0 (*A*), 0.08 (*B*), 0.18 (*C*), 0.3 (*D*). The neuron was at rest without current injection (V_L is set to -70 mV and therefore V is about -72 mV). In each part, *a* and *b* show responses of the neuron model to strong ($I_{app,th} + 0.3\mu$A/cm^2; *a*) and weak ($I_{app,th} + 0.05\mu$A/cm^2; *b*) prolonged stimuli, respectively; $I_{app,th}$ is the minimal I_{app} required to attain spike threshold. The values of $I_{app,th}$ (in μA/cm^2) are 0.84, 0.59, 0.46, and 0.36 for g_{NaP} (in mS/cm^2) values of 0, 0.08, 0.18, and 0.3 respectively. *c* presents the membrane potential in response to a brief (3 ms) current pulse with a density of $I_{app,th} + 2.5\mu$A/cm^2. The values of $I_{app,th}$ in (μA/cm^2) are 7.1, 6.0, 5.3, and 4.7 for g_{NaP} (in mS/cm^2) values of 0, 0.08, 0.18, and 0.3 respectively. - - -, -80 mV. The injected current pulses are indicated below the voltage traces. These currents are always 0 at the starting time. It is evident that increasing g_{NaP} enhances burstiness in the neuron model.

To further characterize the neuron model behavior, we have drawn a map of N_S in bursts evoked by brief (3 ms; Fig. 7*A*) and prolonged (Fig. 7*B*) stimuli in the parameter plane of g_{NaP} and I_{app}. All other parameters were fixed as in the reference parameter set. Brief pulses evoked only a single spike if g_{NaP} was zero or small. As g_{NaP} increased, N_S increased as predicted by the fast-slow analysis. For very large g_{NaP}, the neuron fired many fast and short-amplitude spikes, almost converging to a high plateau, before going back to rest (Fig. 7*A, top right*). The borders of the regimes of 4, 5, 6, etc. spikes were almost independent of I_{app} when it was not too large. This is consistent with the common experimental observation that when I_{app} is brief, N_S is independent of I_{app}. The map for bursts evoked by prolonged current pulses also showed that N_S increases with g_{NaP} (Fig. 7*B*). The parameter I_{app} had a larger impact on N_S in comparison with the case of brief pulses, so that increasing it could raise N_S by one or two spikes.

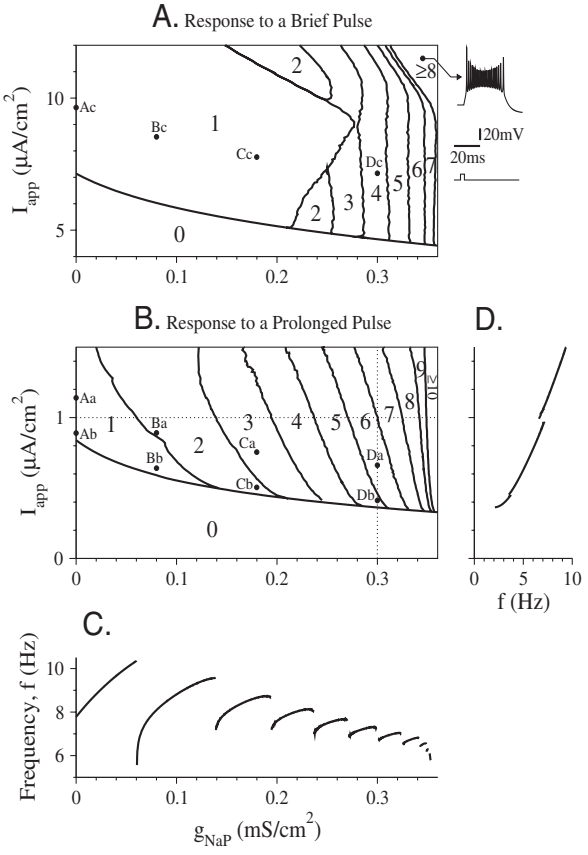

FIG. 7. Modeling: *A* and *B*: dependence of N_S, the number of intraburst spikes, on g_{NaP} and I_{app} for $[Ca^{2+}]_o = 0$. The number in the bounded regions ("2," "1," etc.) denote N_S; "0" denotes no firing. The solid circles denoted by letters, such as "Da," indicate the corresponding panel in Fig. 6. *A*: values of N_S in bursts evoked by brief stimuli. There were 2 discontinuous regimes in which 2 spikes were obtained at low and at high values of I_{app}, whereas only one spike was elicited at intermediate I_{app} regions. The solid circle on the top-right region of map *A* denotes the parameter set of a burst of fast low-amplitude spikes, plotted right to the map. The time course of the applied current is plotted below the voltage time course. *B*: values of N_S in bursts evoked by prolonged stimuli. For a given g_{NaP}, prolonged pulses evoked more intraburst spikes than brief pulses (at least when I_{app} was not extremely large). The dotted lines correspond to the I_{app} and g_{NaP} values for *C* and *D*, respectively. *C*: dependence of the bursting frequency f on g_{NaP} for $I_{app} = 1$ $\mu A/cm^2$. *D*: dependence of the f on I_{app} for $g_{NaP} = 0.3$ mS/cm^2.

We denoted f to be the frequency of periodic bursts evoked by prolonged depolarizations. For a given N_S, f increased as g_{NaP} or I_{app} increased (Fig. 7, *C* and *D*) because the neuron was more excitable. At g_{NaP} or I_{app} values at which N_S increased by 1, f decreased abruptly because more prolonged bursts were followed by larger AHPs.

COMPARING EXPERIMENTAL RESULTS, MODELING, AND THEORY. Increasing g_{NaP} increases N_S and eventually generates bursts with fast, low-amplitude spiking both in the analysis (Fig. 5) and the simulations (Fig. 7). Similarly, blocking g_{NaP} decreases N_S and eventually eliminates bursting in response to prolonged current pulses in the experiments (Fig. 2), the simulations (Figs. 6 and 7) and the mathematical analysis (Fig. 5). The same dependency N_S on g_{NaP} is found experimentally and computationally in response to brief pulses. Furthermore, in response to prolonged pulses, the number of spikes in the first burst is larger than the number of spikes in subsequent bursts in both experiments and simulations.

Role of g_M

Our data (Fig. 3), together with previous data about intact neurons (Yue and Yaari 2004, 2006), show that selective block of I_M markedly enhances the burstiness of CA1 pyramidal cells. These data suggested that I_M normally counteracts the depolarizing drive furnished by I_{NaP}. Hence, it is expected that N_S will increase with I_{NaP} and decrease with I_M. The situation, however, is more complicated because other states appear in the model, as we describe in the following text.

We explored the effects of varying g_{NaP} and g_M at a given I_{app}. In Fig. 8, we present maps of the various states as a function of g_M and g_{NaP}. For brief pulses (Fig. 8*A*), bursting states appeared at intermediate g_{NaP} and g_M values that were not too small. In this bursting regime, N_S increased with g_{NaP} and decreased with g_M. Three other types of patterns appeared for g_{NaP} values above the regimes of single bursts or spikes, denoted by I–III in Fig. 8*A*: I, a fast burst of spikes with decaying amplitudes followed by a high plateau; II, sustained, high-frequency firing; III, an irregular burst with many fast, low-amplitude spikes. The patterns in regimes I and II coexisted with the rest states, namely, the system was bistable in these parameter regimes.

The map obtained for neuronal responses to prolonged stimuli (Fig. 8*B*) was qualitatively similar to the previous map (Fig. 8*A*), although there were some notable differences. First, there were parameter regimes having $N_S = 1$ (regular spiking behavior) that markedly differed in their firing rates. The firing rate in the regime on the right side of the map, denoted by "1_{slow}," was 5–10 Hz, whereas the firing rate in the regime on the left side of the map, denoted by "1_{fast}," was in the order 100 Hz. Second, for $g_{NaP} = 0$, it was possible to obtain a burst of two spikes in a restricted g_M domain. For larger g_{NaP} values, there were two "fingers" in the map where N_S was 2. The finger that extended to the right showed bursting with frequency in the order of 5 Hz. A second finger extending from $g_{NaP} = 0$ to higher g_{NaP} values (adjacent to the "1_{fast}" regime) displayed spiking at a high rate (in the order of 100 Hz) in a doublet manner: the interspike interval alternated between larger and smaller values. Between the two fingers (for g_M values larger

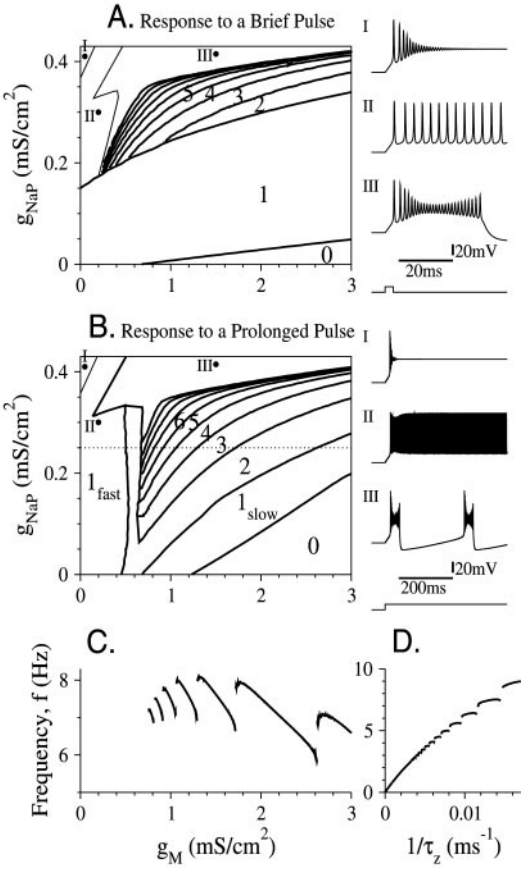

FIG. 8. Modeling. *A* and *B*: dependence of N_S on g_{NaP} and g_M for $[Ca^{2+}]_o$ = 0; τ_z = 75 ms. Symbols are as in Fig. 7. *A*: values of N_S in bursts evoked by brief stimuli with I_{app} = 7 μA/cm^2. Interestingly, N_S could switch abruptly from 1 to a value larger than 2 as g_{NaP} increased. For example, for g_M = 0.8 mS/cm^2, N_S switched from 1 to 3 at g_{NaP} = 0.23 mS/cm^2. *B*: values of N_S in bursts evoked by prolonged stimuli with I_{app} = 1 μA/cm^2. The symbols "1_{fast}" and "1_{slow}" denote tonic firing with fast (interspike interval of order 10 ms) and slow (interspike interval of order 100 ms), respectively. The transition from the parameter regime at which N_S = 2 (left "finger," $g_M \approx 0.6$ mS/cm^2) to the regime of normal bursting was very complex and involved chaotic dynamics. The dotted line denotes the g_{NaP} value used for *C*. The solid circles denoted by I–III in each map represent the parameter sets of the firing patterns shown right to the maps. The time course of the applied current is plotted below the voltage time courses. *C*: dependence of the bursting frequency *f* on g_M. Parameters: I_{app} = 1 μA/cm^2, g_{NaP} = 0.25 mS/cm^2, τ_z = 75 ms. *D*: dependence of the bursting frequency *f* on $1/\tau_z$. Parameters: I_{app} = 1 μA/cm^2, g_{NaP} = 0.25 mS/cm^2, g_M = 1 mS/cm^2.

0.6 mS/cm^2), the neuron exhibited normal bursting for intermediate g_{NaP} values. Three types of patterns, analogous to the patterns obtained for brief pulses, are denoted by I–III in Fig. 8*B*.

To conclude, for both types of stimuli, regular bursts with large N_S appear in a restricted parameter regime with intermediate values of g_{NaP} and g_M, composed of diagonal bands of constant N_S. In this regime, N_S indeed increases with g_{NaP} and decreases with g_M. Several irregular patterns appear outside of this regime.

For a given N_S, *f* generally decreased as g_M increased; At g_M values at which N_S decreased by 1, *f* increased abruptly (Fig. 8*C*). At and above a critical g_M value (3.4 mS/cm^2), the neuron became quiescent (f = 0). As expected from the fast-slow analysis (Table 1, *Eqs. 4* and *5,* Fig. 5), *f* depends linearly on $1/\tau_z$ for large τ_z (Fig. 8*D*). Jumps in *f* occur at moderate values of τ_z at every τ_z value for which N_S increases by 1.

COMPARING EXPERIMENTAL RESULTS, MODELING, AND THEORY. We find that both in the experiment and in the simulations: *1*) blocking g_M increases the N_S evoked by brief stimuli (Figs. 3*A, middle* and *left,* and 8*A*) and eventually transfers the neuron to a bistable tonic firing mode (Figs. 3*A, third panel from left,* and 8*A*). *2*) Blocking g_{NaP} after the g_M blockage causes the neuron to fire only one spike in response to a brief pulse (Figs. 3*A, right,* and 8*A*). *3*) In response to a prolonged pulse, blocking g_M can transfer the neuron to a high plateau depolarization state (Figs. 3*B*, *middle* and *left*; and 8*B*). *4*) If g_{NaP} is also blocked, the neuron fires in a regular mode or becomes quiescent (Figs. 3*B*, *right*; and 8*B*). The conclusions of the analysis that are demonstrated in the simulations (Fig. 8) are *1*) g_M should be strong enough, but not too strong, to obtain bursting, *2*) N_S decreases with g_M, and *3*) *f* is proportional to $1/\tau_z$.

Note that the firing frequency of the real neuron under the effects of both linopirdine and riluzole is of order 10 Hz (Fig. 3*B*), which corresponds to the firing pattern denoted by 1_{slow} in Fig. 8*B* and not to 1_{fast}. In contrast, in the cases in which the neuron bursts in "intact" cells and blocking g_M leads to high plateau, additional blockade of g_{NaP} in the model leads to fast tonic firing. This means that in this respect, the specific example in Fig. 3*B* is different from what is shown in Fig. 8*B*. In reality, but not in the model, the high plateau depolarization eventually decreases and the neuron repolarizes (compare Fig. 3*B*, *middle,* with Fig. 8*B,* I). This is because the model does not include dynamical processes with very slow time scale, such as slow inactivation of I_{NaP} or of I_{Na} (e.g., Fleidervish et al. 1996; French et al. 1990; Mickus et al. 1999).

Effects of varying $[Ca^{2+}]_o$

The analyses described in the preceding text were done in conditions of 0 $[Ca^{2+}]_o$. Here we use the model to interpret intriguing experimental evidence (Su et al. 2001) that reducing $[Ca^{2+}]_o$, but not blocking Ca^{2+} currents and Ca^{2+}-activated K^+ currents, may transfer a nonbursting cell into a burster. Clearly raising $[Ca^{2+}]_o$ will modify the neuronal dynamics by introducing voltage-gated Ca^{2+} currents and Ca^{2+}-activated K^+ currents. In addition, raising $[Ca^{2+}]_o$ will shift the voltage dependence of I_{NaP} activation back toward more positive potentials (Li and Hatton 1996; Yue et al. 2005). Figure 9, *A—C,* illustrates the firing patterns of the neuron model obtained for three sets of parameters (θ_p is the half-maximum potential of the persistent sodium current): g_{Ca} = 0.08 mS/cm^2, θ_p = −41 mV (Fig. 9*A*), g_{Ca} = 0.05 mS/cm^2, θ_p = −44 mV (Fig. 9*B*), and g_{Ca} = 0.02 mS/cm^2, θ_p = −46 mV (Fig. 9*C*). The parameter set in Fig. 9*A* represents parameter values of physiological $[Ca^{2+}]_o$, whereas those in Fig. 9*BC* represent parameters values of reduced $[Ca^{2+}]_o$. The firing pattern of the neuron model obtained for the set g_{Ca} = 0, θ_p = −47 mV, corresponding to $[Ca^{2+}]_o$ = 0, has already been presented in Fig. 6*D*. It can be seen that reducing $[Ca^{2+}]_o$ augments burstiness in this model.

REDUCING $[CA^{2+}]_O$ IS NOT EQUIVALENT TO BLOCKING CA^{2+} CURRENTS. Maps showing N_S values in bursts evoked by brief and prolonged current pulses as a function of θ_p and a second parameter related to the Ca^{2+}-gated currents or Ca^{2+}-activated K^+ currents, are shown in Fig. 10. Increasing g_{Ca} with all Ca^{2+}-activated K^+ currents blocked ($g_C = g_{sAHP}$ = 0) aug-

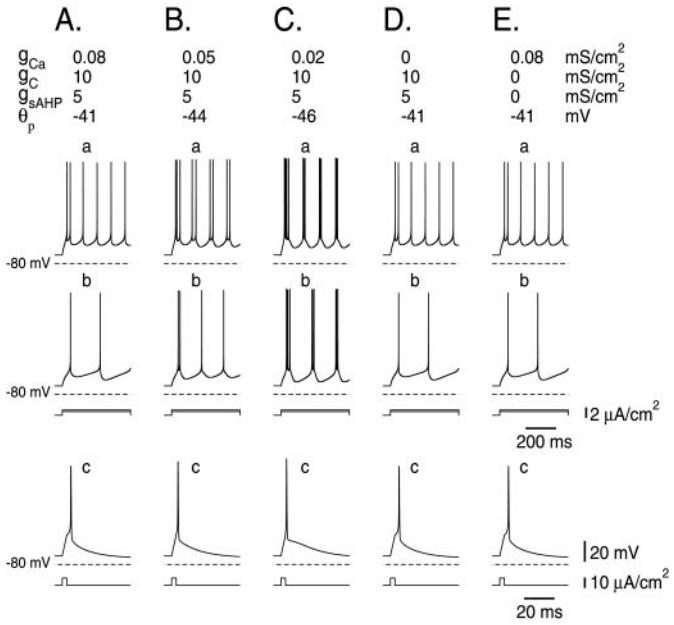

FIG. 9. Modeling: variant firing patterns of the neuron model for different values of $[Ca^{2+}]_o$. The sets of parameters $\{g_{Ca}$ (mS/cm^2), g_C (mS/cm^2), g_{sAHP} (mS/cm^2), θ_p (mV)$\}$ are *A*: {0.08, 10, 5, −41}. *B*: {0.05, 10, 5, −44}. *C*: {0.02, 10, 5, −46}. *D*: {0, 10, 5, −46}. *E*: {0.08, 0, 0, −41}. The parameter sets *A–C* mimic gradual reduction of $[Ca^{2+}]_o$ from the physiological level *A* through *B* and *C*; when $[Ca^{2+}]_o$ becomes 0, the parameter set {0, 10, 5, −47} is equal to that of Fig. 6*D* and is not shown here again. The parameter set *D* mimics blockade of Ca^{2+} conductance. The parameter set *E* mimics Ca^{2+} buffering, which eliminates Ca^{2+}-dependent K^+ currents. The neuron model is at rest before the current injection. Each column in the figure includes 3 voltage traces. The panels in *a* and *b* show the responses of the neuron model to prolonged strong and weak stimuli, respectively. *c* show the responses of the neuron model to brief (3 ms) stimuli. The horizontal dashed line represents −80 mV. The waveforms of the stimuli are provided below the voltage trace(s). Stimulus intensities are 1 μA/cm^2 for *a*, 0.7 μA/cm^2 for *b,* and 7 μA/cm^2 for *c*. Reducing $[Ca^{2+}]_o$ (*A–C*), but neither blocking g_{Ca} (*D*) nor blocking g_C and g_{sAHP} (*E*), induces bursting in a regular firing cell.

mented N_S for both brief and prolonged stimuli (Fig. 10, *A* and *B*) and weakly reduced *f* (Fig. 10*C*). To assess the effects of Ca^{2+}-activated K^+ conductances, we set g_{Ca} = 0.08 mS/cm^2 and computed N_S as a function of θ_p and either g_C or g_{sAHP}. As expected, increasing g_C suppressed burstiness and decreased N_S for a specific value of θ_p (Fig. 10, *D* and *E*); *f* increased with g_C (Fig. 10*F*). Increasing g_{sAHP} within the range of the parameter we used (from 0 to 20 mS/cm^2) did not affect N_S substantially (data not shown). This finding is expected because the I_{sAHP} is slow, and the burst is terminated by I_M before I_{sAHP} becomes strong enough to have a considerable effect.

When Ca^{2+}-activated K^+ conductances were intact, the effect of varying g_{Ca} on N_S depended on g_C. The value of N_S increased with g_{Ca} for small g_C values and decreased with g_{Ca} for large g_C values. Figure 10, *G—I,* demonstrates that with our reference parameter set (g_C = 10 mS/cm^2, g_{sAHP} = 5 mS/cm^2), the hyperpolarizing effect of g_C dominated, N_S decreased with g_{Ca} for both brief and prolonged stimuli, and *f* increased with g_{Ca}.

The increase in burstiness on reducing $[Ca^{2+}]_o$ resulted mainly from the decrease in θ_p. However, the decrease of g_{Ca} per se also could affect N_S. Although in most cases blocking g_{Ca} did not change N_S (e.g., Fig. 9*D* and points 9A and 9D in Fig. 10*H*), there were also conditions in which blocking g_{Ca} transferred the system to a higher level of burstiness (for example, when g_{Ca} = 0.2 mS/cm^2 and θ_p = −45 mV, Fig. 10*H*). Similarly, although blocking g_C did not lead to bursting for our reference parameter set (Fig. 9*E*), it could increase N_S for lower values of θ_p (Fig. 10, *D* and *E*). For brief stimuli, bursting was obtained for more hyperpolarized values of θ_p in comparison to the case of prolonged stimuli. Therefore evoking bursts with brief stimuli required lower values of $[Ca^{2+}]_o$ than evoking bursts with prolonged stimuli.

COMPARING BETWEEN EXPERIMENTAL AND MODELING RESULTS. We observed both in experiments (Fig. 1) and in the simulations (Figs. 6*D,* 9, *A—C,* and 10, *G* and *H*) that reducing $[Ca^{2+}]_o$ increases the propensity for bursting in response to brief and prolonged stimuli and augments N_S. The neuron model also mimicked two more experimental results obtained in CA1 pyramidal neurons: blocking Ca^{2+} currents pharmacologically, which also blocks Ca^{2+}-activated K^+ currents, or blocking the latter currents only (by injecting a fast Ca^{2+} buffer into the neuron), did not change the regular firing mode

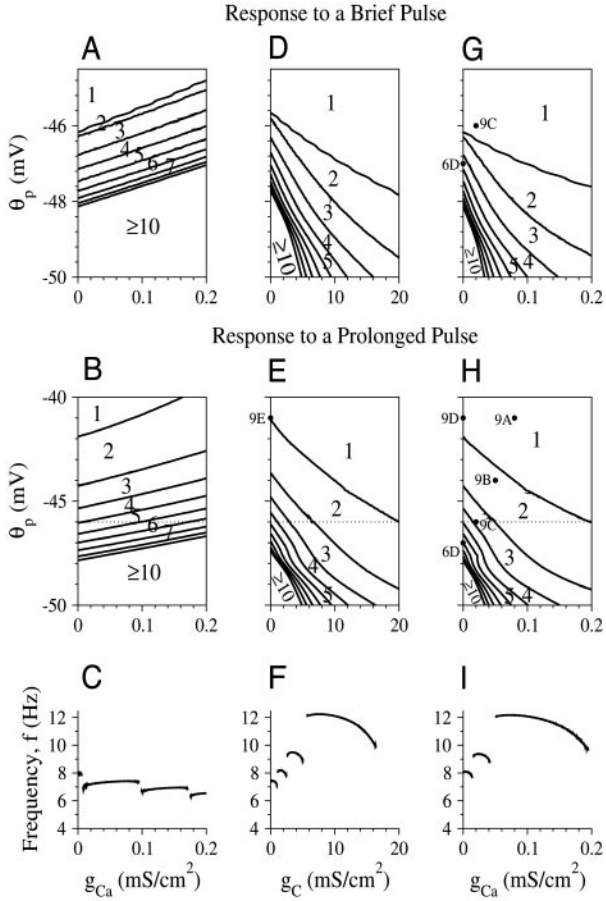

FIG. 10. Modeling. *Top* and *middle*: dependence of N_S on either g_{Ca} or g_C and θ_p. Symbols are as in Fig. 7. *Top*: response to a brief pulse with I_{app} = 7 μA/cm^2. *Middle*: response to a prolonged pulse with I_{app} = 1 μA/cm^2. *Bottom*: dependence of the bursting frequency *f* on either g_{Ca} or g_C for I_{app} = 1 μA/cm^2 and θ_p = −46 mV. *A* and *B*, N_S vs. g_{Ca} and θ_p for g_C = g_{sAHP} = 0. *C*: *f* vs. g_{Ca} for g_C = g_{sAHP} = 0. *D* and *E*. N_S vs. g_C and θ_p plane for g_{Ca} = 0.08 mS/cm^2, g_{sAHP} = 0. *F*: *f* vs. g_C for g_{Ca} = 0.08 mS/cm^2, g_{sAHP} = 0. *G* and *H*: N_S vs. g_{Ca} and θ_p for for g_C = 10 mS/cm^2, g_{sAHP} = 5 mS/cm^2. *I*: *f* vs. g_{Ca} for g_C = 10 mS/cm^2, g_{sAHP} = 5 mS/cm^2. In all the panels, N_S increases as θ_p is hyperpolarized. The solid circles in panels *E*, *G*, and *H* denoted by "9" or "6" and letters, such as "9A," indicate the corresponding column in Figs. 9 or 6, respectively.

of these neurons (Su et al. 2001). Examples are shown in Fig. 9*D*, in which g_{Ca} is set to 0 (other parameters, including θ_p, are as in Fig. 9*A*), and in Fig. 9*E*, where both g_C and g_{sAHP} are set to 0. It can be seen in these figures that blocking Ca^{2+}-activated K^+ currents in either way does not modify the firing behavior of the neuron model for the chosen parameter set.

DISCUSSION

Major conclusions

Our finding that truncated neurons fire in a similar manner to intact neurons in both normal and low $[Ca^{2+}]_o$ allowed us to use a single-compartment model to analyze the underlying mechanism of bursting. Our analysis leads to several conclusions: first, CA1 pyramidal cells can burst via a single-compartment mechanism with one slow variable, namely the activation variable of I_M (z), provided two conditions are fulfilled, *1*) The kinetics of the spike generating currents (i.e., I_{Na} and I_{Kdr}) are fast, although not too fast and *2*) the activation curve of I_M is properly tuned. If it is too depolarized, the neuron will fire tonically; if it is too hyperpolarized, the neuron will be quiescent. Accordingly, it was shown experimentally that shifting the activation curve of I_M toward more negative potentials with retigabine (Tatulian et al. 2001; Wickenden et al. 2000) suppresses bursting behavior in both normal and 0 $[Ca^{2+}]_o$ (Yue and Yaari 2004).

Second, moderate values of g_{NaP} favor burstiness because it enhances bistability of the fast subsystem. Thus N_S increases with g_{NaP}. Assuming a natural heterogeneity in g_{NaP}, the model can replicate the diversity of intrinsic firing patterns found experimentally (Fig. 6), but if g_{NaP} is too large, the neuron will display prolonged bursts with many low-amplitude spikes or a high plateau depolarization (Figs. 7 and 8). Bistability and bursting, however, can be supported also by the window I_{Na} provided it is sufficiently large (not shown). Therefore the presence of g_{NaP} is not a necessary condition for bursting in our model.

Third, g_M is mandatory for bursting in 0 $[Ca^{2+}]_o$. This feature of the model is consistent with our experimental findings showing that blocking g_M with linopirdine converts bursting in 0 $[Ca^{2+}]_o$ to plateau depolarization (Fig. 3). Conversely, increasing g_M decreases N_S. Ultimately, when g_M is large enough, the neuron does not fire spikes. When $[Ca^{2+}]_o$ is elevated, I_{sAHP} and I_M play a similar role in the neuronal dynamics, with I_{sAHP} being slower.

Fourth, our model predicts that shifting the activation curve of I_{NaP} to more negative potentials will increase burstiness (Fig. 10). Given that such a shift is obtained by lowering $[Ca^{2+}]_o$ (Li and Hatton 1996; Yue et al. 2005), the model readily accounts for the experimental finding that lowering $[Ca^{2+}]_o$, but not blocking Ca^{2+} and Ca^{2+}-activated conductances, induces bursting behavior in regular spiking CA1 pyramidal cells (Su et al. 2001).

Comparison between experimental and modeling results

The dynamics of the neuron model have been compared with the dynamics of native neurons from several aspects.

1. CAN WE OBTAIN IN THE MODEL THE VARIETY OF FIRING PATTERNS RECORDED EXPERIMENTALLY? We have shown in Figs. 6 and 4*B* that by varying g_{NaP} and V_L the model can mimic the various firing parameters obtained in $[Ca^{2+}]_o = 0$ (see Fig. 1 in Su et al. 2001). In reality, there is biological heterogeneity in other parameters as well that may contribute to the variety of firing patterns. Similarly, the model can mimic the firing patterns obtained experimentally at various levels of $[Ca^{2+}]_o$, g_{Ca}, and g_C (compare Fig. 9 with Fig. 1 here and Fig. 2 in Sue et al. 2001).

2. HOW DOES THE PROPENSITY FOR BURSTING AND N_S VARY WITH I_{app}, g_{NaP}, AND g_M? In the neuron model (Fig. 7) as well as in native neurons (Fig. 2), N_S increases with g_{NaP} and depends only weakly on I_{app}. When the neuron bursts, N_S decreases with g_M (Fig. 8) (see Fig. 1 in Yue and Yaari 2004) and reaches a fast tonic firing state or a high plateau for low levels of g_M (Figs. 3 and 8).

3. HOW DOES THE PROPENSITY FOR BURSTING AND N_S VARY WITH g_{Ca}, g_C, AND $[Ca^{2+}]_o$? It has been reported that reducing $[Ca^{2+}]_o$, but not blocking the Ca^{2+} current or Ca^{2+}-activated K^+ currents, increases the propensity for bursting and N_S (see Figs. 3, 7, and 8 in Sue et al. 2001). This experimental observation can be replicated in the model (Fig. 10) using certain parameter sets and the assumption that elevating $[Ca^{2+}]_o$ causes θ_p to shift to more positive voltage. Figure 10 suggests that in principle, however, there may be cases in which N_S increases with the blockade of g_C (Fig. 10, *D* and *E*) or g_{Ca} (Fig. 10, *G* and *H*).

DISCREPANCIES BETWEEN MODELING AND EXPERIMENTAL RESULTS. The dynamical equations of the model do not include slow processes (>1 s). Therefore the model cannot explain slow changes observed experimentally, such as the slow repolarization of the membrane potential during a high plateau and the resumption of spiking (Fig. 3, *middle*).

In this paper, we show several diagrams in which N_S varies as a function of two parameters (Figs. 7, 8, and 10). When a third parameter is varied, the relative positions of the areas of particular N_S values may shift. The two-dimensional diagrams provide therefore qualitative information about the type of transition that may occur when parameters vary, but one cannot expect that the experimental behavior will always follow the two-dimensional diagrams quantitatively. For example, Fig. 8*B* shows that in response to a prolonged pulse, reducing g_M may transfer a bursting pattern to a high plateau, and further reduction of g_{NaP} may transfer a high plateau neuron to a neuron spiking at high rates. Figure 8*B* does not overlap the example of Fig. 3, in which g_M blockade by linopirdine followed by g_{NaP} blockade by riluzole transfers a bursting pattern to a high plateau and then to a tonic firing pattern (with firing frequency of ~10 Hz). It is possible, however, that linopirdine and riluzole, used to blocked g_M and g_{NaP}, respectively, exert additional effects on neuronal excitability. Note that Fig. 3*A* is consistent with Fig. 8*A* regarding the effects of blocking g_M and g_{NaP} on the firing patterns in response to a brief current pulse. In both cases, blocking g_M in the case of bursting neurons can bring the neuron to a fast spiking state leading to a high plateau, and subsequent blockade of g_{NaP} leads to firing of one spike only.

For the model, we chose a θ_h value that is ~20 mV depolarized compared with available voltage-clamp experimental measurements (Colbert and Pan 2002; Gasparini and Magee 2002; Martina and Jonas 1997), to obtain a large enough window I_{Na} to support bistability in the fast subsystem.

Window I_{Na} is needed for bursting and even for spiking in previous models as well and is obtained by assuming a small value of $\theta_m - \theta_h$ (e.g., 4.2 mV in Pinsky and Rinzel 1994; Traub and Miles 1991; Traub et al. 1991) or by assuming a very large g_{Na} value in the axo-somatic compartment (Mainen and Sejnowski 1996).

Comparison with other models of bursting neurons

A 16-compartmental model of CA1 pyramidal cells, albeit with passive dendrites, was provided by Shuai et al. (2003). This model also displayed rhythmic bursting in zero $[Ca^{2+}]_o$. The reversal potential of the leak current in the soma was −58 mV, more depolarized than the value we used (−70 mV). The reversal potential of the leak current in the dendrites, however, was assumed to be 0 mV (*Eq. 2* in Shuai et al. 2003), without any apparent biological reason. Simulating their model (using parameters of Table 1, Shuai et al. 2003), we found that after disconnecting the soma from the apical dendrite their respective resting potentials were −63.9 and 0 mV. Bursting in the intact neuron model depended on depolarization of the soma by the dendrite and disappeared after disconnecting the soma from the dendritic compartments. This behavior of the latter neuron model is incongruent with our experimental data showing that bursting behavior persists in truncated neurons (Figs. 1, 2, 3, and 4*A*).

The kinetics of ionic currents in the model of Shuai et al. (2003) also differed considerably from ours. Most notably, the activation time constant of I_{NaP} in their model was 30 ms even though experimental measurements have shown it to be well below 1 ms (Kay et al. 1998; Magistretti et al. 2003; Vervaeke et al. 2006). In contrast, I_{NaP} activation kinetics in our model is fast, and z is the only slow variable. Consequently, bistability of the fast subsystem of variables is needed to generate bursting behavior.

In other models of hippocampal and neocortical pyramidal neurons, intrinsic bursting in normal $[Ca^{2+}]_o$ was attributed to a ping-pong interplay between fast Na^+ and K^+ currents in the soma and slow Ca^{2+} and K^+ (mostly Ca^{2+}-dependent) currents in the apical dendrites (Bazhenov et al. 2004; Mainen and Sejnowski 1996; Pinsky and Rinzel 1994; Traub and Miles 1991; Traub et al. 1991). The latter mechanism depends on the coupling between soma and apical dendrites; bursting behavior was not obtained when coupling resistance was too small or too large.

The CA1 pyramidal cell has widely branched basal dendrites, which are electrotonically compact (Zador et al. 1995). In general, the electrotonic separation between the axon, the soma and the basal dendrite may modify the firing patterns of the neuron. The existence of a slow current, such as I_M, and bistability of the fast subsystem, will be needed for bursting even in models similar to ours where the spatial structure of the truncated dendrite is explicitly considered. Effects of the electrotonic separation between soma and axon can be addressed theoretically as more data about the axon becomes available.

Predictions for future experiments

The major results and predictions of the model, such as the increase of N_S with g_{NaP} and its decrease with g_M and the generation of high plateaus, have been confirmed experimentally as reported here and elsewhere (Gilles et al. 1999; Su et al. 2001; Yue and Yaari 2004, 2006). The model yields several more predictions. For example, increasing g_{NaP} ultimately will lead to prolonged bursts with many low-amplitude spikes (Fig. 8) or to high-plateau depolarization. Also, increasing g_{Ca} in normal $[Ca^{2+}]_o$ will moderately decrease the propensity for bursting when Ca^{2+}-activated K^+ currents are operative and strong enough and will moderately increase this propensity when these currents are blocked (Figs. 9 and 10). It would be interesting to test these predictions by modulating these various currents pharmacologically or by simulating changes in these currents using the dynamic-clamp technique (Sharp et al. 1993; Vervaeke et al. 2006).

Functional implications

Our experimental and computational results suggest that bursting in adult CA1 pyramidal cells in zero and in low $[Ca^{2+}]_o$ in vitro is generated by a "square-wave" mechanism, i.e., from interplay between ionic currents located within one compartment, namely, the soma/axon initial segment. Thus separation between fast currents in the soma/axon initial segment and slow currents in the apical dendrites (the ping-pong mechanism) is not obligatory for bursting. However, the latter mechanism may be invoked in adult CA1 pyramidal cells by blocking I_A pharmacologically after which backpropagating spikes evoke dendritic Ca^{2+} spikes that, in turn, trigger somatic bursting (Magee and Carruth 1999). A similar ping-pong mechanism may exist naturally in developing CA1 pyramidal cells (Chen et al. 2005). Thus CA1 pyramidal cells may display both square-wave and ping-pong bursting, depending on their developmental stage and on the composition of the extracellular milieu. Interestingly, although it has been established that pyramidal neurons in cortical layer V can display a ping-pong bursting behavior in some conditions (Larkum et al. 1999), they can also burst after most of their apical dendrites are truncated (A. E. Telfeian and B. W. Connors, personal communication). Thus the square-wave mechanism described here for CA1 pyramidal cells may be relevant for those neurons also.

Hippocampal pyramidal cells in vivo were shown to alternate between regular firing ("simple" spikes) and burst firing ("complex" spikes), depending on the behavioral state of the animal (Ranck 1973). It is not yet known how intrinsic factors contribute to complex spike bursting in vivo. However, decreases in $[Ca^{2+}]_o$, which occur during synchronized neuronal activity (Heinemann et al. 1977) and may attain levels of ≤0.2 mM during epileptic seizures (Pumain et al. 1985), are expected to induce square-wave bursting in CA1 pyramidal cells in vivo. Likewise, factors that upmodulate g_{NaP} (e.g., hypoxia or the accumulation of nitric oxide) (Hammarstrom and Gage 2002), or downmodulate g_M (e.g., a variety of neurotransmitters) (Brown and Yu 2000), also are likely to enhance this mode of bursting in these neurons in vivo.

ACKNOWLEDGMENTS

We thank Y. Mandelblat for technical assistance, J. Rinzel for helpful discussions, and C. Meunier for careful reading of the manuscript. D. Golomb thanks the Mathematical Biosciences Institute where part of this research was done.

GRANTS

The research was supported by Israel Science Foundation Grant 311/04, Binational U.S.-Israel Science Foundation Grants 2003019 to D. Golomb and 200323001 to Y. Yaari, Deutsche Forschungsgemeinschaft Grant SFB TR3, the German-Israel collaborative research program of the Bundesministerium für Bildung und Forschung (BMBF) and the Ministry of Science and Technology (MOST), and the Henri J. and Erna D. Leir Chair for Research in Neurodegenerative Diseases (Y. Yaari).

REFERENCES

Azouz R, Jensen MS, and Yaari Y. Ionic basis of spike after-depolarization and burst generation in adult rat hippocampal CA1 pyramidal cells. *J Physiol* 492: 211–223, 1996.

Bazhenov M, Timofeev I, Steriade M, and Sejnowski TJ. Potassium model for slow (2–3 Hz) in vivo neocortical paroxysmal oscillations. *J Neurophysiol* 92: 1116–1132, 2004.

Bertram R, Butte MJ, Kiemel T, and Sherman A. Topological and phenomenological classification of bursting oscillations. *Bull Math Biol* 57: 413–439, 1995.

Borg-Graham L. Interpretations of data and mechanisms for hippocampal pyramidal cell models. In: *Cereberal Cortex*, *Cortical Models*, edited by Ulinski PS, Jones EG, and Peters A. New York: Plenum, 1999, vol. 13, p. 19–138.

Brown BS and Yu SP. Modulation and genetic identification of the M channel. *Prog Biophys Mol Biol* 73: 135–166, 2000.

Cantrell AR, Ma JY, Scheuer T, and Catterall WA. Muscarinic modulation of sodium current by activation of protein kinase C in rat hippocampal neurons. *Neuron* 16: 1019–1026, 1996.

Chao TI and Alzheimer C. Effects of phenytoin on the persistent Na^+ current of mammalian CNS neurons. *Neuroreport* 6: 1778–1780, 1995.

Chen S, Yue C, and Yaari Y. A transitional period of calcium-dependent bursting triggered by spike backpropagation into apical dendrites in developing hippocampal neurons. *J Physiol* 567: 79–93, 2005.

Colbert GM and Pan E. Ion channel properties underlying axonal action potential initiation in pyramidal neurons. *Nat Neurosci* 5: 533–538, 2002.

Ermentrout B. *Simulating, Analyzing, and Animating Dynamical Systems: A Guide to XPPAUT for Researchers and Students (Software, Environment, Tools*). Philadelphia: Society for Industrial and Applied Mathematics, 2002.

Fleidervish IA, Friedman A, and Gutnick MJ. Slow inactivation of Na^+ current and slow cumulative spike adaptation in mouse and guinea-pig neocortical neurons in slices. *J Physiol* 493: 83–97, 1996.

French CR, Sah P, Buckett KJ, and Gage PW. A voltage-dependent persistent sodium current in mammalian hippocampal neurons. *J Gen Physiol* 95: 1139–1157, 1990.

Gasparini S and Magee JC. Phosphorylation-dependent differences in the activation properties of distal and proximal dendritic Na^+ channels in rat CA1 hippocampal neurons. *J Physiol* 541: 665–672, 2002.

Gilles N, Blanchet C, Shichor I, Zaninetti M, Lotan I, Bertrand D, and Gordon D. A scorpion alpha-like toxin that is active on insects and mammals reveals an unexpected specificity and distribution of sodium channel subtypes in rat brain neurons. *J Neurosci* 19: 8730–8739, 1999.

Golomb D and Amitai Y. Propagating neuronal discharges in neocortical slices: computational and experimental study. *J Neurophysiol* 78: 1199–1211, 1997.

Gu N, Vervaeke K, Hu H, and Storm JF. Kv7/KCNQ/M and HCN/h, but not $K_{Ca}2$/SK channels, contribute to the somatic medium after-hyperpolarization and excitability control in CA1 hippocampal pyramidal cells. *J Physiol* 566: 689–715, 2005.

Halliwell JV and Adams PR. Voltage-clamp analysis of muscarinic excitation in hippocampal neurons. *Brain Res* 250: 71–92, 1982.

Hammarstrom AK and Gage PW. Hypoxia and persistent sodium current. *Eur Biophys J* 31: 323–330, 2002.

Harris KD, Hirase H, Leinekugel X, Henze DA, and Buzsáki G. Temporal interaction between single spikes and complex spike bursts in hippocampal pyramidal cells. *Neuron* 32: 141–149, 2001.

Heinemann U, Lux HD, and Gutnick MJ. Extracellular free calcium and potassium during paroxsmal activity in the cerebral cortex of the cat. *Exp Brain Res* 27: 237–243, 1977.

Hoffman DA, Magee JC, Colbert CM, and Johnston D. K^+ channel regulation of signal propagation in dendrites of hippocampal pyramidal neurons. *Nature* 387: 869–853, 1997.

Hoppensteadt FC and Izhikevich EM. *Weakly Connected Neural Networks*. New York: Springer-Verlag, 1997.

Izhikevich EM. Neural excitability, spiking and bursting. *Int J Bifurcation Chaos* 10: 1171–1266, 2000.

Izhikevich EM. *Dynamical Systems in Neuroscience: The Geometry of Excitability and Bursting.* Cambridge MA: MIT Press, 2007.

Izhikevich EM, Desai NS, Walcott EC, and Hoppensteadt FC. Bursts as a unit of neural information: selective communication via resonance. *Trends Neurosci* 26: 161–167, 2003.

Jensen MS, Azouz R, and Yaari Y. Variant firing patterns in rat hippocampal pyramidal cells modulated by extracellular potassium. *J Neurophysiol* 71: 831–839, 1994.

Jung HY, Staff NP, and Spruston N. Action potential bursting in subicular pyramidal neurons is driven by a calcium spike aftercurrent. *J Neurosci* 21: 3312–3321, 2001.

Karst H, Jöels M, and Wadman WJ. Low-threshold calcium current in dendrites of the adult rat hippocampus. *Neurosci Lett* 164: 154–158, 1993.

Kay AR, Sugimori M, and Llinás R. Kinetic and stochastic properties of a persistent sodium current in mature guinea pig cerebellar Purkinje cells. *J Neurophysiol* 80: 1167–1179, 1998.

Kay AR and Wong RKS. Calcium current activation kinetics in isolated pyramidal neurones of the CA1 region of the mature guinea-pig hippocampus. *J Physiol* 392: 603–616, 1987.

Lancaster B and Adams PR. Calcium-dependent current generating the afterhyperpolarization of hippocampal neurons. *J Neurophysiol* 55: 1268–1282, 1986.

Larkum ME, Zhu JJ, and Sakmann B. A new cellular mechanism for coupling inputs arriving at different cortical layers. *Nature* 398: 338–341, 1999.

Li Z and Hatton GI. Oscillatory bursting of phasically firing rat supraoptic neurones in low-Ca^{2+} medium: Na^+ influx, cytosolic Ca^{2+} and gap junction. *J Physiol* 496: 379–394, 1996.

Lisman JE. Bursts as a unit of neural information: making unreliable synapses reliable. *Trends Neurosci* 20: 38–43, 1997.

Maccaferri G and McBain CJ. The hyperpolarization-activated current (Ih) and its contribution to pacemaker activity in rat CA1 hippocampal stratum oriens-alveus interneurons. *J Physiol* 497: 119–130, 1996.

Madison DV and Nicoll RA. Control of the repetitive discharge of rat CA1 pyramidal neurons in vitro. *J Physiol* 354: 319–331, 1984.

Magee JC. Dendritic hyperpolarization-activated currents modify the integrative properties of hippocampal CA1 pyramidal neurons. *J Neurosci* 18: 7613–7624, 1998.

Magee JC and Carruth M. Dendritic voltage-activated ion channels regulate the action potential firing mode of hippocampal CA1 pyramidal neurons. *J Neurophysiol* 82: 1895–1901, 1999.

Magistretti J, Ragsdale DS, and Alonso A. Kinetic diversity of single-channel burst openings underlying persistent Na^+ current in entorhinal cortex neurons. *Biophys J* 85: 3019–3034, 2003.

Mainen ZF and Sejnowski TJ. Influence of dendritic structure on firing pattern in model neocortical neurons. *Nature* 382: 363–366, 1996.

Mandelblat Y, Etzion Y, Grossman Y, and Golomb D. Period doubling of calcium spike firing in a model of a Purkinje cell dendrite. *J Comput. Neurosci* 11: 43–62, 2001.

Martina A and Jonas P. Functional differences in Na^+ channel gating between fast-spiking interneurons and principal neurones of rat hippocampus. *J Physiol* 505: 593–603, 1997.

Martina A, Schultz JH, Ehmke H, Monyer H, and Jonas P. Functional and molecular differences between voltage-activated K^+ channels of fast-spiking interneourns and pyramidal neurons of rat hippocampus. *J Neurosci* 18: 8111–8125, 1998.

Metz AE, Jarsky T, Martina M, and Spruston N. R-type calcium channels contribute to afterdepolarization and bursting in hippocampal CA1 pyramidal neurons. *J Neurosci* 25: 5763–5773, 2005.

Mickus T, Jung H, and Spruston N. Properties of slow, cumulative sodium channel inactivation in rat hippocampal CA1 pyramidal neurons. *Biophys J* 76: 846–860, 1999.

Pinsky PF and Rinzel J. Intrinsic and network rhythmogenesis in a reduced Traub model for CA3 neurons. *J Comput Neurosci* 1: 39–60, 1994.

Pumain R, Menini C, Heinemann U, Louvel J, and Silva-Barrat C. Chemical synaptic transmission is not necessary for epileptic seizures to persist in the baboon *Papio papio. Exp Neurol* 89: 250–258, 1985.

Ranck JB Jr. Studies on single neurons in dorsal hippocampal formation and septum in unrestrained rats. I. Behavioral correlates and firing repertoires. *Exp Neurol* 41: 461–531, 1973.

Rinzel J and Ermentrout GB. Analysis of neural excitability and oscillations. In: *Methods in neuronal modeling: From Ions to Networks*, (2nd ed.), edited by Koch C and Segev I. Cambridge, MA: MIT Press, 1998, p. 251–291.

Rush ME and Rinzel J. The potassium A-current, low firing rates, and rebound excitation in Hodgkin-Huxley models. *Bull Math Biol* 57: 899–929, 1995.

Sah P, Gibb AJ, and Gage PW. Potassium current activated by depolarization of dissociated neurons from adult guinea pig hippocampus. *J Gen Physiol* 92: 263–278, 1988a.

Sah P, Gibb AJ, and Gage PW. The sodium current underlying action potentials in guinea pig hippocampal CA1 neurons. *J Gen Physiol* 91: 373–398, 1988b.

Schnee ME and Brown BS. Selectivity of linopirdine (DuP 996), a neurotransmitter release enhancer, in blocking voltage-dependent and calcium-activated potassium currents in hippocampal neurons. *J Pharmacol Exp Ther* 286: 709–717, 1998.

Schwartzkroin PA. Characteristics of CA1 neurons recorded intracellularly in the hippocampal in vitro slice preparation. *Brain Res* 85: 423–436, 1975.

Sharp AA, O'Neil MB, Abbott LF, and Marder E. The dynamic clamp: artificial conductances in biological neurons. *Trends Neurosci* 16: 389–394, 1993.

Shuai J, Bikson M, Hahn PJ, Lian J, and Durand DM. Ionic mechanisms underlying spontaneous CA1 neuronal firing in Ca^{2+}-free solution. *Biophys J* 84: 2099–2011, 2003.

Spadoni F, Hainsworth AH, Mercuri NB, Caputi L, Martella G, Lavaroni F, Bernardi G, and Stefani A. Lamotrigine derivatives and riluzole inhibit $I_{Na,P}$ in cortical neurons. *Neuroreport* 13: 1167–1170, 2002.

Spain WJ, Schwindt PC, and Crill WE. Anomalous rectification in neurons from cat sensorimotor cortex in vitro. *J Neurophysiol* 57: 1555–1576, 1987.

Stocker M, Krause M, and Pedarzani P. An apamin-sensitive Ca^{2+}-activated K^+ current in hippocampal pyramidal neurons. *Proc Natl Acad Sci USA* 96: 4662–4667, 1999.

Storm JF. Action potential repolarization and a fast after-hyperpolarization in rat hippocampal pyramidal cells. *J Physiol* 385: 733–759, 1987.

Su H, Alroy G, Kirson ED, and Yaari Y. Extracellular calcium modulates persistent sodium current-dependent burst-firing in hippocampal pyramidal neurons. *J Neurosci* 21: 4173–4182, 2001.

Tatulian L, Delmas P, Abogadie FC, and Brown DA. Activation of expressed KCNQ potassium currents and native neuronal M-type potassium currents by the anti-convulsant drug retigabine. *J Neurosci* 21: 5535–5545, 2001.

Terman D. The transition from bursting to continuous spiking in excitable membrane model. *J Nonlinear Sci* 2: 135–182, 1992.

Thompson SM and Wong RK. Development of calcium current subtypes in isolated rat hippocampal pyramidal cells. *J Physiol* 439: 671–689, 1991.

Traub RD, Jefferys JGR, Miles R, Whittington MA, and Tóth K. A branching dendritic model of a rodent CA3 pyramidal neurone. *J Physiol* 481: 79–95, 1994.

Traub RD and Miles R. *Neuronal networks of the hippocampus.* New York: Cambridge, 1991.

Traub RD, Wong RK, Miles R, and Michelson H. A model of a CA3 hippocampal pyramidal neuron incorporating voltage-clamp data on intrinsic conductances. *J Neurophysiol* 66: 635–649, 1991.

Urbani A and Belluzzi O. Riluzole inhibits the persistent sodium current in mammalian CNS neurons. *Eur J Neurosci* 12: 3567–3574, 2000.

Vasilyev DV and Barish ME. Postnatal development of the hyperpolarization-activated excitatory current I_h in mouse hippocampal pyramidal neurons. *J Neurosci* 22: 8992–9004, 2002.

Vervaeke K, Hu H, Graham LJ, and Storm JF. Contrasting effects of the persistent Na^+ current on neuronal excitability and spike timing. *Neuron* 49: 257–270, 2006.

Wang HS, Pan Z, Shi W, Brown BS, Wymore RS, Cohen IS, Dixon JE, and McKinnon D. KCNQ2 and KCNQ3 potassium channel subunits: Molecular correlates of the M-channel. *Science* 282: 1890–1893, 1998.

Warman EN, Durand DM, and Yuen GL. Reconstruction of hippocampal CA1 pyramidal cell electrophysiology by computer simulations. *J Neurophysiol* 71: 2033–2045, 1994.

Wickenden AD, Yu W, Zou A, Jegla T, and Wagoner PK. Retigabine, a novel anti-convulsant, enhances activation of KCNQ2/Q3 potassium channels. *Mol Pharmacol* 58: 591–600, 2000.

Wong RK and Prince DA. Afterpotential generation in hippocampal pyramidal cells. *J Neurophysiol* 45: 86–97, 1981.

Yaari Y and Beck H. "Epileptic neurons" in temporal lobe epilepsy. *Brain Pathol* 12: 234–239, 2002.

Yue C, Remy S, Su H, Beck H, and Yaari Y. Proximal persistent Na^+ channels drive spike afterdepolarizations and associated bursting in adult CA1 pyramidal cells. *J Neurosci* 25: 9704–9720, 2005.

Yue C and Yaari Y. KCNQ/M channels control spike afterdepolarization and burst generation in hippocampal neurons. *J Neurosci* 24: 4614–4624, 2004.

Yue C and Yaari Y. Axo-somatic and apical dendritic Kv7/M channels differentially regulate the intrinsic excitability of adult rat CA1 pyramidal cells. *J Neurophysiol* 95: 3480–3495, 2006.

Zador AM, Agmon-Snir H, and Segev I. The morphoelectrotonic transform: a graphical approach to dendritic function. *J Neurosci* 15: 1669–1682, 1995.